1 Title: Modulation of flight and feeding behaviours requires presynaptic IP_3Rs in dopaminergic
2 neurons

3 Authors: Anamika Sharma and Gaiti Hasan

4 National Centre for Biological Sciences, TIFR, Bangalore – 560065

5 For correspondence: gaiti@ncbs.res.in

Abstract:

Innate behaviours, though robust and hard wired, rely on modulation of neuronal circuits, for eliciting an appropriate response according to internal states and external cues. *Drosophila* flight is one such innate behaviour that is modulated by intracellular calcium release through inositol 1,4,5-trisphosphate receptors (IP_3Rs). Cellular mechanism(s) by which IP_3Rs modulate neuronal function for specific behaviours remain speculative, in vertebrates and invertebrates. To address this, we generated an inducible dominant negative form of the IP_3R (IP_3R^{DN}). Flies with neuronal expression of IP_3R^{DN} exhibit flight deficits. Spatiotemporal expression of IP_3R^{DN} helped identify key flight-modulating dopaminergic neurons with axonal projections in the mushroom body. Attenuation of IP_3R function in these presynaptic dopaminergic neurons resulted in flies with shortened flight bouts and a disinterest in seeking food, accompanied by reduced excitability and dopamine release upon cholinergic stimulation. Our findings suggest that the same neural circuit modulates the drive for food search and for undertaking longer flight bouts.

Introduction:

The Inositol-1, 4, 5-trisphosphate receptor (IP_3R) is an Endoplasmic Reticulum (ER) resident ligand-gated calcium (Ca^{2+}) channel found in metazoans. In neurons, the IP_3R is activated through multiple classes of signaling molecules that include neuromodulators such as neuropeptides, neurotransmitters and neurohormones. Studies from ex-vivo vertebrate neurons have identified a role for the IP_3R in multiple cellular processes including regulation of neurite growth (Takei et al., 1998; Xiang et al., 2002), synaptic plasticity (Fujii et al., 2000; Nishiyama et al., 2000) and more recently pre-synaptic neurotransmitter release (Gomez et al., 2020). However, the relevance of IP_3-mediated signaling mechanisms to cellular processes and subsequent behavioural and neurophysiological outputs need better understanding. In non-excitable cells Ca^{2+} release through the IP_3R regulates a range of cellular events including growth, secretion (Inaba et al., 2014), gene expression (Ouyang et al., 2014) and mitochondrial function (Cárdenas et al., 2010, Bartok et al., 2019). In excitable cells such as neurons, identifying cellular functions of the IP_3R is more complex because in addition to IP_3-mediated Ca^{2+} release, there exist several plasma-membrane localised ion channels that bring in extracellular Ca^{2+} in response to neurotransmitters and changes in membrane excitability.

Three IP_3R isotypes, IP_3R1, 2 and 3 are encoded by mammalian genomes (Furuichi et al., 1994; Taylor et al., 1999). Of these, IP_3R1 is the most prevalent isoform in neurons and is relevant in the context of several neurodegenerative disorders (Terry et al., 2019). Human mutations in IP_3R1 cause Spinocerebellar ataxia 15 (SCA15), SCA29 and Gillespie syndrome (Hasan & Sharma, 2020). Disease causing IP_3R1 mutations span different domains but several are clustered in the amino terminal IP_3 binding region, from where they impact ER-Ca^{2+} release when tested in mammalian cell lines (Ando et al., 2018) . A common feature of these neurological disorders is loss of motor-coordination or ataxia. The ataxic symptoms

arise primarily from malfunction and/or degeneration of cerebellar Purkinje neurons where the IP_3R1 is expressed abundantly in the soma, dendrites and axons. Dendritic expression of the IP_3R in Purkinje neurons determines Long Term Depression (LTD), a form of post-synaptic plasticity (Miyata et al., 2000). Interestingly, a recent study in *Drosophila* also identified the IP_3R as an essential component of post-synaptic plasticity, required for decoding the temporal order of a sensory cue and a reward stimulus, in neurons of a higher brain centre, the Mushroom Body (Handler et al., 2019). Somatic expression of the IP_3R very likely contributes to maintenance of cellular Ca^{2+} homeostasis (Berridge, 2016) . A pre-synaptic role for the IP_3R has been demonstrated in the *Drosophila* neuromuscular junction (Shakiryanova et al., 2011), motor neurons (Klose et al., 2010) and most recently in axonal projections of Purkinje neurons (Gomez et al., 2020). Physiological and behavioural significance of pre-synaptic IP_3/Ca^{2+} signals in either case however remain speculative.

To understand how IP_3R alters neuronal function and related neurophysiology and behaviour we have in the past studied several mutants for the single IP_3R gene (*itpr*) in *Drosophila melanogaster* (Joshi et al., 2004). The *Drosophila* IP_3R shares 60% sequence identity, similar domain organisation, biophysical and functional properties with mammalian IP_3Rs(Chakraborty & Hasan, 2012; Srikanth & Hasan, 2004). Several hypomorphic and heteroallelic combinations of *Drosophila* IP_3R mutants are viable and exhibit flight deficits ranging from mild to strong, the focus of which lies in aminergic neurons (Banerjee et al., 2004). However, such mutants do not easily allow cell specific attenuation of IP_3R function. In this context, a dominant-negative mutant form of mammalian IP_3R1, generated recently, abrogated IP_3R function in mammalian cell lines (Alzayady et al., 2016). The mammalian dominant negative IP_3R1 gene was based on the finding that all monomers in the IP_3R tetramer need to bind IP_3 for channel opening (Alzayady et al., 2016). Failure of a single IP_3R monomer to bind IP_3 renders the resultant IP_3R tetramer non-functional. *Drosophila* IP_3Rs are also tetrameric suggesting that a similar strategy for generating a dominant-negative IP_3R could be used for cell-specific studies of neuronal function and behaviour. Consequently we generated and characterised a *Drosophila* IP_3R dominant negative (IP_3R^{DN}) transgene. Cell-specific expression of *Drosophila* IP_3R^{DN} allowed the identification of two pairs of flight modulating dopaminergic neurons. Neuromodulatory signals received by these neurons stimulate IP_3/Ca^{2+} signals to regulate critical aspects of pre-synaptic cellular physiology with significant impact on flight and feeding behaviour.

77 RESULTS:

78 ***Ex vivo* characterization of a dominant negative IP_3R:**

79 To understand how Ca^{2+} release through IP_3R affects cellular properties of neurons,
80 we designed a mutant *itpr* cDNA to function as a dominant negative upon overexpression in
81 wild type *Drosophila* neurons. The dominant negative construct (*Itpr*^{DN}) was designed based
82 on previous studies in mammalian IP_3Rs (Figure 1A, B; Alzayady et al., 2016). Three
83 conserved basic residues in the ligand binding domain (R272, K531 and Q533) of the
84 *Drosophila* IP_3R cDNA were mutated to Glutamine (Q) and the resultant mutant cDNA was
85 used to generate GAL4/UAS inducible transgenic strains (*UASItpr*^{DN}) as described in methods.
86 Expression from the *Itpr*^{DN} construct was validated by western blots of adult fly head lysates.
87 IP_3R levels were significantly enhanced in fly heads with *Itpr*^{DN} as compared to genetic
88 controls and were equivalent to overexpression of a wild-type IP_3R transgene (*Itpr*$^{+}$*;* Figure
89 1C). IP_3-mediated calcium release from the IP_3R in the presence of *Itpr*^{DN}, was tested on
90 previously characterised glutamatergic interneurons in the larval ventral ganglion known to
91 respond to the muscarinic acetylcholine receptor (mAChR) ligand Carbachol. These neurons
92 can be marked with a GAL4 strain (*vGlut*^{VGN6341}; Jayakumar et al., 2016; 2018). Changes in
93 cytosolic calcium were measured by visualising Ca^{2+} dependent fluorescence changes of a
94 genetically encoded Ca^{2+} sensor GCaMP6m (Chen et al., 2013) in *ex vivo* preparations.
95 *vGlut*^{VGN6341} marked neurons expressing IP_3R^{DN} exhibit reduced as well as delayed Ca^{2+}
96 responses to Carbachol stimulation as compared to controls (Figure 1D). Ca^{2+}- released from
97 the IP_3R is also taken up by mitochondria (Bartok et al., 2019). Hence we measured
98 mitochondrial Ca^{2+} uptake post Carbachol stimulation using mitoGCaMP, a mitochondrial
99 targeted fluorescence sensor for Ca^{2+} (Lutas et al., 2012). Similar to cytosolic GCaMP,
100 attenuated Ca^{2+} responses were observed upon carbachol stimulation in presence of IP_3R^{DN}
101 (Figure 1E). Interestingly, the mitochondrial response did not exhibit a delay in reaching peak
102 values. We attribute the residual Ca^{2+} release observed in the cytosol and mitochondria to
103 the persistence of some IP_3R tetramers with all four wild type subunits, encoded by the
104 native *itpr* gene. In summary, both cytosolic and mitochondrial Ca^{2+} measurements
105 confirmed the efficacy of the *Drosophila* IP_3R^{DN} for attenuating IP_3-mediated Ca^{2+} release
106 from ER stores upon GPCR stimulation in *Drosophila* neuron

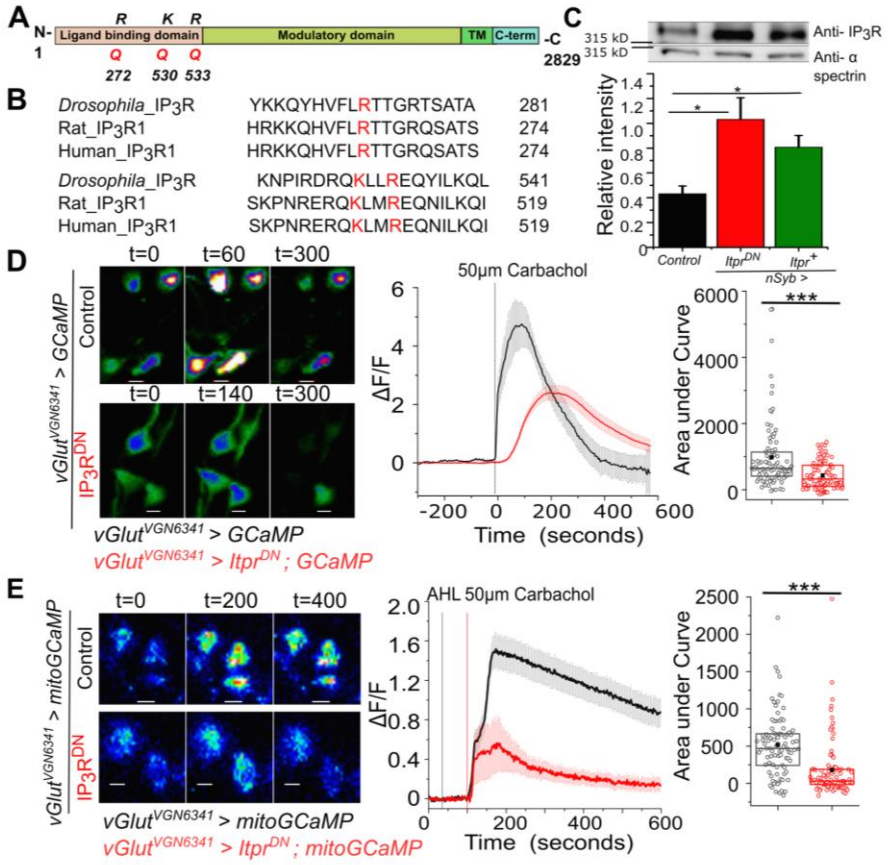

Figure 1: Generation and characterisation of a dominant negative IP_3R (IP_3R^{DN})

A. Domain organization of the *Drosophila* IP_3R. The Arginine (R) and Lysine (K) residues mutated to Glutamine (Q) to generate a dominant-negative IP_3R (IP_3R^{DN}) are shown.
B. Alignment of the Drosophila IP_3R with Rat IP_3R1 and Human IP_3R1 in the region of the mutated amino acids. All three residues (red) are conserved.
C. Significantly higher immuno-reactivity against the IP_3R is observed upon pan-neuronal (*nsybGAL4)* expression of IP_3R^{DN} (*UASItpr^{DN}*) and IP_3R (*UASItpr^{+}*) in adult heads. Statistical comparison was made with respect to *Canton S* as control, n=5, *p< 0.05 (Mann-Whitney U test).
D. Representative images show changes in cytosolic Ca^{2+} in larval neurons of the indicated genotypes as judged by GCaMP6m fluorescence at the indicated time intervals after stimulation with Carbachol (Scale bars indicate 5 µm). Warmer colors denote increase in $[Ca^{2+}]_{cyt}$. Mean traces of normalized GCaMP6m fluorescence in response to Carbachol (4s/frame) in *vGlut^{VGN6341}GAL4* marked neurons, with (red) and without (black) IP_3R^{DN} (ΔF/F ± SEM) (middle panel). Area under the curve (right) was quantified from 0 - 420s from the traces in the middle. *vGlut^{VGN6341}GAL4 > UAS GCaMP* N = 6 brains, 92 cells; *vGlut^{VGN6341}GAL4 > UAS Itpr^{DN}; UAS GCaMP* N = 6 brains, 95 cells. ***p< 0.005 (Two tailed Mann-Whitney U test).
E. Representative images show changes in mitochondrial Ca^{2+} in larval neurons of the indicated genotypes as judged by mitoGCaMP6m fluorescence at the indicated time intervals after stimulation with Carbachol (Scale bars indicate 5 µm). Warmer colors denote increase in $[Ca^{2+}]_{cyt}$. Mean traces of normalized mitoGCaMP6m fluorescence in response to Carbachol (2s/frame) in *vGlut^{VGN6341}GAL4* marked neurons, with (red) and without (black) IP_3R^{DN} (ΔF/F ± SEM) (middle panel). Area under the curve (right) was quantified from 100 - 400s from the traces in the middle. *vGlut^{VGN6341}GAL4 > UAS mitoGCaMP* N = 5 brains, 89 cells; *vGlut^{VGN6341}GAL4 > UAS Itpr^{DN}; UAS mitoGCaMP* N = 5 brains, 88 cells. ***p< 0.005 (Two tailed Mann-Whitney U test).

The IP_3R is required in a subset of central dopaminergic neurons for maintenance of *Drosophila* flight*:*

Next we tested the functional efficacy of $Itpr^{DN}$ for attenuating neuronal function in *Drosophila.* From previous reports we know that *itpr* mutants are flightless and their flight deficit can be rescued partially by overexpression of a wild-type cDNA construct ($Itpr^{+}$; Venkatesh et al., 2001) in monoaminergic neurons (Banerjee, 2004). Subsequent studies identified mild flight deficits upon RNAi mediated knock down of the IP_3R in dopaminergic neurons (DANs) (Pathak et al., 2015) when tethered flight was tested for 30 seconds. Knock-down of the IP_3R in serotonergic neurons, that form another major subset of the tested monoaminergic neurons, did not give a flight deficit (Sadaf et al., 2012). Here we tested if pan-neuronal expression of the IP_3R^{DN} affects longer flight bout durations in a modified tethered flight assay lasting for 15 mins (see methods and Manjila & Hasan, 2018). Flies with pan-neuronal *nsybGAL4* driven expression of $Itpr^{DN}$ exhibit significantly reduced flight bouts (281.4±38.9s) as compared to the appropriate genetic controls $Itpr^{DN}/+$ (773.3±30.4s) and *nsyb/+* (670.6±41.3s) (Figure 2- figure supplement 1A). Stronger deficits in flight bout durations (185.2±33.7 seconds) were obtained by expression of $Itpr^{DN}$ in Tyrosine Hydroxylase expressing cells, that include a majority of dopaminergic neurons (*THGAL4*; Friggi-Grelin et al., 2003), as well as in a dopaminergic neuron subset (260±30.5 s) marked by *THD'GAL4* (Liu et al., 2012) (Figure 2A, 2B). As additional controls the same GAL4 drivers were tested with overexpression of $Itpr^{+}$. Interestingly, flight deficits were also observed upon overexpression of $Itpr^{+}$ across all neurons (*nsyb>*$Itpr^{+}$; 410±31.6s; Figure 2- figure supplement 1A), all TH expressing cells (*TH>*$Itpr^{+}$; 482.2±41.4s) and a dopaminergic neuron subset, (*THD'>*$Itpr^{+}$; 433.5±35.6s; Figure 2A), though these were milder than with expression of $Itpr^{DN}$.

To confirm that shorter flight bouts in flies expressing $Itpr^{DN}$ are a consequence of reduced IP_3R function in dopaminergic neurons and not an overexpression artefact, we expressed a previously validated *Itpr* RNAi (Agrawal et al., 2010) and recorded flight durations in an identical flight assay. Significantly reduced flight bouts, comparable to the flight deficits obtained upon expression of $Itpr^{DN}$, were observed by knockdown of the IP_3R with *nsybGAL4*, *THGAL4* and *THD'GAL4* (Figure 2A, Figure 2- figure supplement 1A, Figure 2-figure supplement 2). These data confirm that IP_3R function is necessary in the *THD'* marked subset of dopaminergic neurons for maintenance of flight bouts. Further, it suggests that either decrease ($Itpr^{DN}$ and *Itpr RNAi*) or increase ($Itpr^{+}$) of IP_3-mediated Ca^{2+} release in *THD'* neurons affects flight bout durations.

As an independent test of IP_3R requirement, the wild-type IP_3R was overexpressed in dopaminergic neurons of an adult viable IP_3R mutant, $itpr^{ka1091/ug3}$ or $itpr^{ku}$ (Joshi et al., 2004). Overexpression of the IP_3R in monoaminergic neurons of *itpr* mutants can rescue free flight measured for short durations of 5-10 secs (Banerjee, 2004). Short (30s, Figure 2-figure supplement 1B) and long (900s; Figure 2C) flight bouts were measured in a heteroallelic viable *itpr* mutant combination $itpr^{ku}$, with $Itpr^{+}$ overexpression in all neurons or in dopaminergic neurons and dopaminergic neuronal subsets . Pan-neuronal overexpression of

173 the IP_3R (*nsyb>Itpr*$^{+}$) rescued short flight bouts partially in 10 out of 30 flies tested (Figure 1-
174 figure supplement 1B). Interestingly, complete rescue of short flight was observed in flies
175 rescued by IP_3R overexpression in dopaminergic neurons and their TH-D subsets but not the
176 TH-C' subset *(*Figure 2 - figure supplement 1B). Better rescue by IP_3R overexpression in
177 dopaminergic neurons suggests weak expression of *nSybGAL4* in dopaminergic neurons,
178 though this idea needs further verification. When tested for longer flight bouts, a partial
179 rescue from dopaminergic neurons and TH-D subsets was observed (304.2±25.1s; *TH>Itpr+*)
180 as compared to control flies (747.8±19.4s; Figure 2C), suggesting that the IP_3R regulates
181 flight bout durations from both dopaminergic and certain non-dopaminergic neurons
182 (Agrawal et al., 2010). The *TH-D* and *TH-C GAL4*s express in anatomically distinct central
183 dopaminergic neurons of which the *THD1GAL4* and *THD'GAL4* uniquely mark the PPL1 and
184 PPM3 DAN clusters. Taken together, shorter flight bouts in *THD>Itpr*^{DN} flies and significant
185 rescue of flight by *THD>Itpr*$^{+}$ overexpression in flightless *itpr*^{ku} identifies an essential
186 requirement for IP_3R function in the PPL1 and/or PPM3 DANs for flight bouts lasting upto
187 ~300s.
188 The two PPL1 clusters on each side of the brain consist of 12 pairs of neurons (Mao &
189 Davis, 2009) and have been implicated in the maintenance of long flight bouts previously
190 (Pathak et al., 2015). To further restrict flight modulating neuron/s in the PPL1 group we
191 identified split*GAL4* strains that mark fewer PPL1 neuron/s and project to individual lobes of
192 the Mushroom Body (MB; Figure 2- figure supplement 1C and Figure 2D) (Aso et al., 2014;
193 Aso & Rubin, 2016). Amongst the identified split*GAL4* strains, flight deficits were observed
194 by expression of IP_3R^{DN} in PPL1 DANs projecting to the MB lobes α'2α2, α3, γ1peduncle and
195 γ2α'1 (*MB504BGAL4*), but not with PPL1 DANs projecting to the MB lobes α'2α2, α3 and
196 Y1peduncle (*MB438BGAL4*; Figure 2E), suggesting PPL1-γ2α'1DANs as the primary focus of
197 IP_3R function. Indeed, expression of *Itpr*^{DN} in PPL1-γ2α'1 DANs, marked by *MB296BGAL4,*
198 resulted in significantly shorter flight bouts, when compared to *Itpr*$^{+}$ expression in the same
199 cells (Figure 2E). Expression of *Itpr*^{DN} in other PPL1 neurons failed to exhibit significant flight
200 deficits (Figure 2 - figure supplement 1D). Thus *PPL1-γ2α'1* DANs require IP_3R function to
201 sustain longer flight bouts. These data do not exclude a role for the IP_3R in PPM3 DANs that
202 are also marked by *THD'GAL4* in the context of flight.

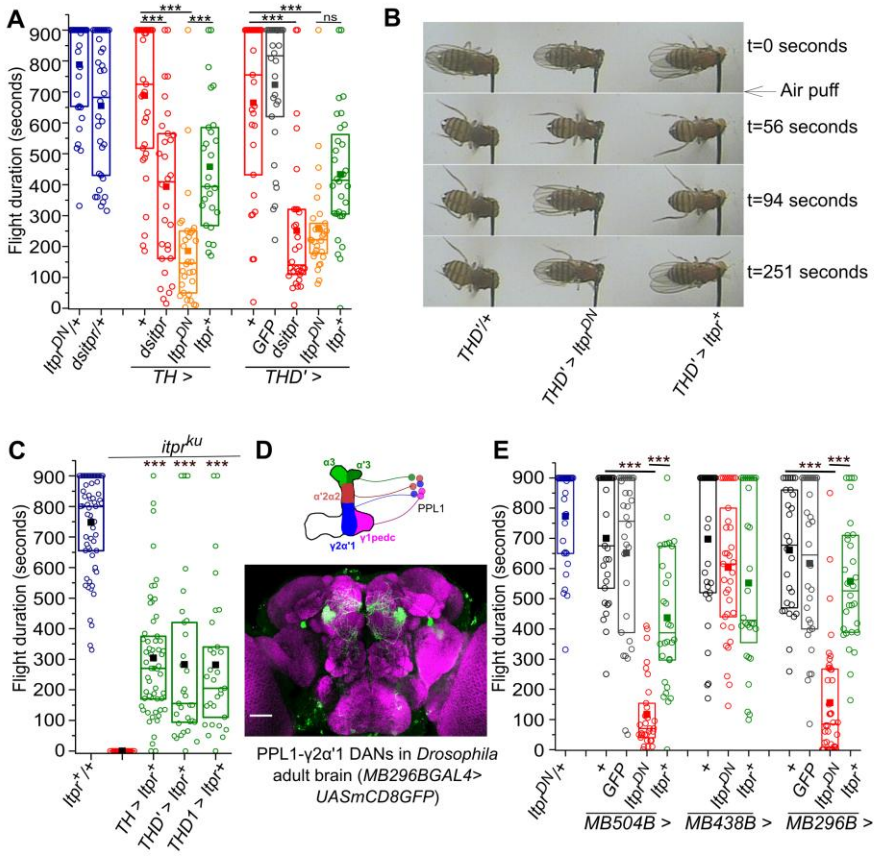

203

204 **Figure 2:** The IP_3R is required in central dopaminergic neurons for maintaining long flight bouts.

205 A. Flight deficits observed in flies expressing IP_3R RNAi (*dsitpr*), IP_3R^{DN} (*Itpr*^{DN}) and IP_3R^{WT} (*Itpr*$^{+}$) across all
206 dopaminergic and TH expressing cells (*TH*) as well as a subset of dopaminergic neurons (*THD'*). Flight
207 times of flies of the indicated genotypes are represented as box plots where the box represents 25-
208 75% of the distribution, each circle is the flight time of an individual fly, the small filled square
209 represents mean flight time and the horizontal line is the median. Flight was tested in flies with GFP in
210 *THD'* marked neurons as an over-expression control.
211 B. Snapshots from flight videos of air puff stimulated flight bouts in the indicated genotypes at the
212 specified time points.
213 C. Box plots (as in A above) represent flight bout durations of control and *itpr* mutant flies (*itpr*^{ku}).
214 Expression of a wild-type cDNA for the IP_3R (*UAS Itpr*$^{+}$) with indicated dopaminergic *GAL4s* rescued
215 flight to a significant extent.
216 D. A schematic of PPL1 DANs projecting to different lobes of one half of the mushroom body (top); An
217 adult brain with GFP expression (green) driven by *MB296BGAL4*. GFP expression is restricted to PPL1-
218 γ2α'1 neurons and the γ2α'1 MB lobe. The brain neuropil is immunostained with anti Brp (purple).
219 Scale bar = 50 µm.
220 E. Box plots (as in A) of flight bout durations in flies expressing IP_3R^{DN} (*Itpr*^{DN}) and IP_3R^{WT} (*Itpr*$^{+}$) in the
221 indicated *PPL1 DAN* splitGAL4 strains.

222 In all box plots n > 25, ***p< 0.005 **p< 0.01 , n.s., not significant at p < 0.05 by two-tailed Student's t test
223 (for C) or one-way ANOVA followed by post hoc Tukey's test (for A and E). Comparisons for significance were
224 with the control values except where marked by a horizontal line.

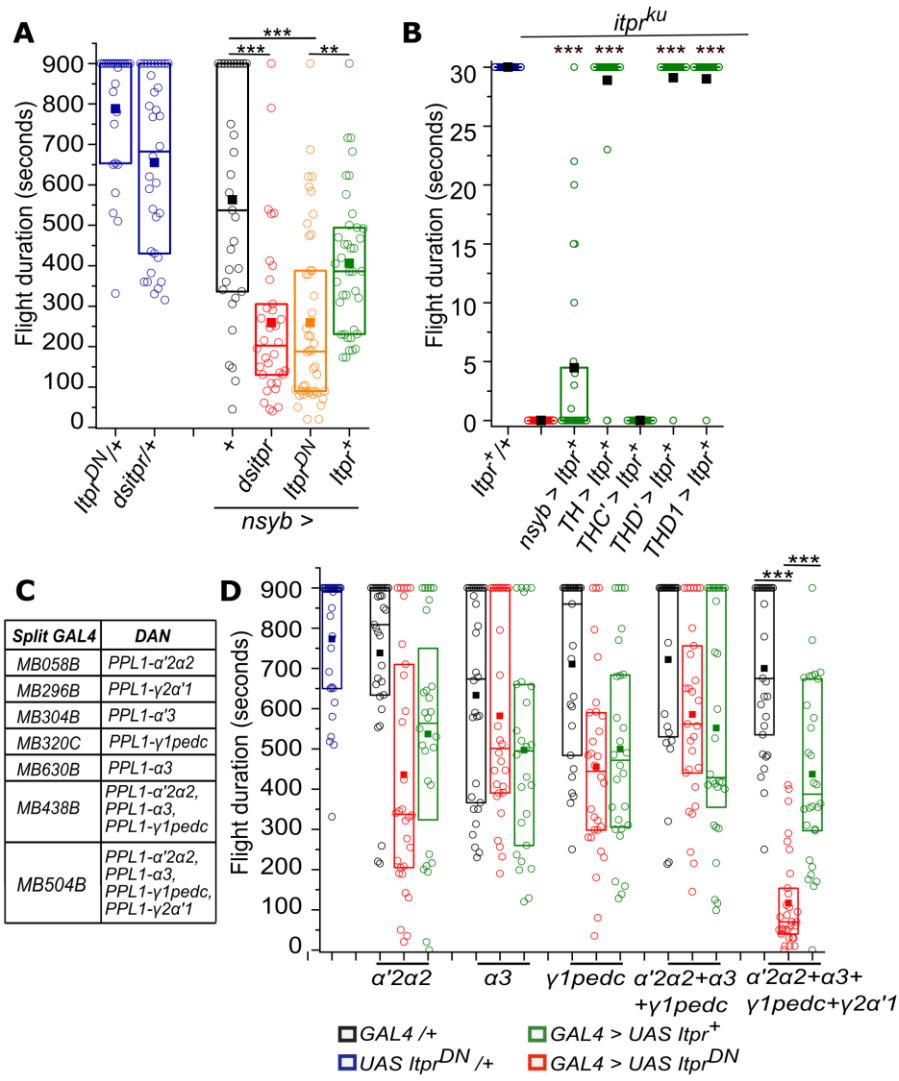

Figure 2- figure supplement 1: Perturbation of IP_3R signaling in neurons affects the duration of flight bouts.

A) Box plots represent flight deficits observed upon perturbing IP_3R signaling after expressing IP_3R RNAi (*dsitpr*), IP_3R^{DN} (*Itpr*^{DN}) and IP_3R^{WT} (*Itpr*$^{+}$) across all classes of neurons with *nsybGAL4.*

B) Box plots represents flight bout durations of *itpr* mutant flies measured for 30 seconds, upon expression of *UAS Itpr*$^{+}$ with the indicated *GAL4s.*

C) SplitGAL4 strains used to label subsets of PPL1 DANs.

D) Box plots represent flight bout durations of flies upon perturbing IP_3R signaling after expressing IP_3R^{DN} (*Itpr*^{DN}) and IP_3R^{WT} (*Itpr*$^{+}$) in the indicated *PPL1 DAN* expressing strains.

Box plot symbols are as described in methods and Figure 2A; n ≥ 30, ***p< 0.005 **p< 0.05, n.s., not significant at p < 0.05 by two-tailed Student's t test (for B) or one-way ANOVA followed by post hoc Tukey's test (for A and D. All comparisons for significance were with the control values except where marked by a horizontal line. Comparisons for significance were with *itpr* mutants in B.

Figure 2- figure supplement 2: Video showing flight defect in *THD'> Itpr*^{DN} (Right) as compared to control (*THD'/+,* Left)

240 **The IP_3R is required in a late developmental window for adult flight:**

241 Shorter flight bouts in adults might arise either due to loss or change in properties of
242 identified neurons during development. Alternately, the IP_3R might acutely affect the
243 function of these neurons during flight in adults. To distinguish between these possibilities
244 we employed the TARGET system (McGuire et al., 2003) for temporal control of IP_3R^{DN}
245 expression in *PPL1* and *PPM3* DANs. TARGET uses a ubiquitously expressed temperature
246 sensitive repressor of GAL4 (Tub-GAL80^{ts}) that allows GAL4 expression at 29°, but not at
247 lower temperatures. Hence expression of a GAL4 driven *UAS* transgene can be controlled by
248 changing incubation temperatures from 18° to 29°. *THD'GAL4* driven *Itpr^{DN}* expression was
249 restricted to the larval stages (data not shown), 0-48h after puparium formation (APF), 48-
250 96h APF and for 0-3 days in adults. Flight deficits were observed upon expression of IP_3R^{DN}
251 during pupal development and not when expressed in adults. In pupae the deficit was most
252 prominent by expression of the *Itpr^{DN}* during the shorter window of 48-96hr APF (Figure 3A).

253 Requirement for the IP_3R during the 48-96hr APF window was independently
254 confirmed by measuring flight after temporal expression of *Itpr$^+$* in dopaminergic neurons of
255 *itpr^{ku}* (Figure 3B). Flight in *itpr^{ku}* mutant animals was rescued to a significant extent by *Itpr$^+$*
256 expression from 48-96h APF (277±60.3s) but not when expressed before and after.
257 Interestingly, post-48 hr APF is also the time period during which levels of the IP_3R are
258 upregulated in the pupal brain (Figure 3C). Thus expression from the *Itpr^{DN}* encoding
259 transgene during the 48-96hr interval presumably results in the formation of a majority of
260 inactive IP_3R tetramers due to the presence of at least one IP_3R^{DN} monomer. The cellular and
261 physiological consequences of inactive IP_3Rs in pupal, and subsequently adult brains, was
262 investigated next.

263 It is known that specification of central dopaminergic neurons is complete in late
264 larval brains (Hartenstein et al., 2017) The number of PPL1 DANs was no different between
265 controls and in flies expressing *Itpr^{DN}* in either *TH-D* or *MB296B* marked neurons (Figure 3 -
266 figure supplement 1A). This finding agrees with our observation that larval expression of
267 *Itpr^{DN}* had no effect on adult flight. Moreover projections from *MB296B* to the *γ2α'1* MB
268 lobes also appeared unchanged upon expression of *Itpr^{DN}* (Figure 3 - figure supplement 1B).

269 To understand the nature of signaling through the IP_3R, required during pupal
270 development we tested flight after knockdown of an IP_3/Ca^{2+} linked GPCR, the muscarinic
271 acetylcholine receptor (mAChR). From a previous study it is known that neuronal expression
272 of the mAChR during pupal development is required for adult flight (Agrawal et al., 2013).
273 Adult flight bouts were significantly shorter upon stage specific knock-down (48-96h APF) of
274 the mAChR in TH-D' neurons with an RNAi under temporal control of the TARGET system
275 (Figure 3D). Further knockdown of mAChR in PPL1- *γ2α'1* DANs also manifested mild flight
276 defect (Figure 3 - figure supplement 1C). These data suggest that the mAChR and IP_3-
277 mediated Ca^{2+} release are required during pupal maturation of a central brain circuit that
278 functions for the maintenance of long flight bouts. Alternately, the pupal requirement may
279 arise from the fact that both the IP_3R (Figure 3A, B) and the mAChR (Figure 3D) are
280 synthesized in late pupal neurons, carried over to adult neurons where they have a slow

281 turnover, and function during acute flight. Taken together our data support the idea that
282 acetylcholine, a neurotransmitter, activates the mAChR on PPL1 DANs of late pupae and/or
283 adults to stimulate Ca^{2+} release through the IP_3R. Cellular changes arising from loss of IP_3
284 mediated Ca^{2+} release were investigated next.

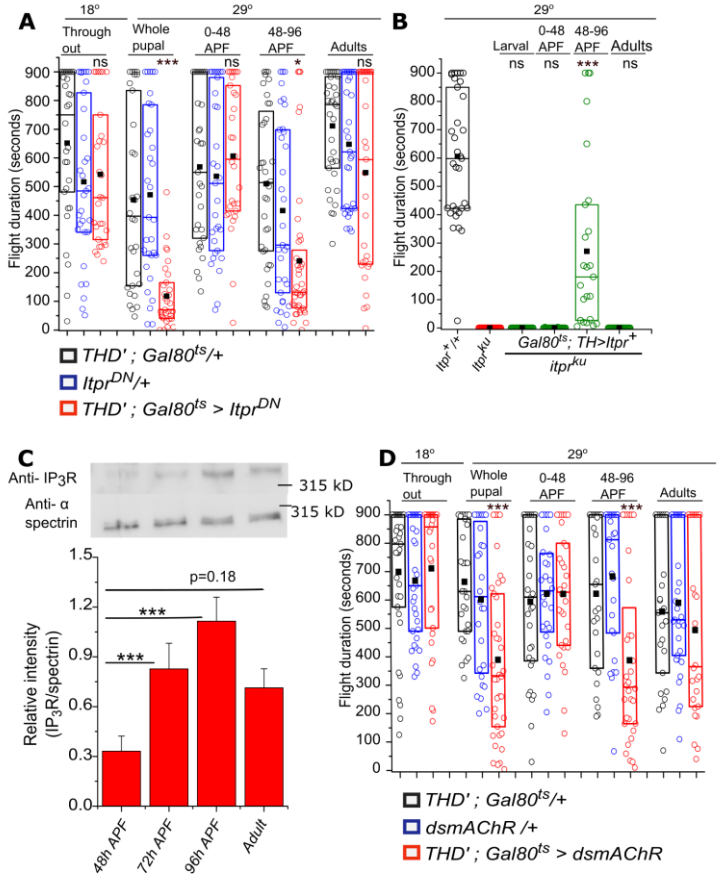

Figure 3: Adult flight phenotypes arise from late pupal expression of the IP_3R and mAChR

A) Box plots of flight bout durations in adults after temporal expression of IP_3R^{DN} in *THD'* neurons (*THD'; TubGAL80^{ts} > Itpr^{DN}*) by transferring them to 29˚C at the indicated stages of development. For adult expression, flies were transferred to 29˚C immediately after eclosion and tested for flight after 3 days.

B) Box plots of flight bout durations after expressing the IP_3R (*Itpr^{+}*) in dopaminergic cells of *itpr* mutants at the indicated stages of development. For stage specific expression a *TH; TubGAL80^{ts}* strain was used and the progeny transferred to 29˚C at appropriate time developmental points.

C) Levels of the IP_3R increase in late pupae between 72-96 hrs APF and plateau between 96hrs APF and adults (3 days). A representative western blot from lysates of dissected central nervous systems of *Canton S* probed with anti-IP_3R and anti-spectrin is shown (top). Three independent lysates and blots were quantified (below). ***p< 0.005, t-test.

D) Box plots with flight bout durations of adult flies after knockdown of the Muscarinic acetylcholine receptor (mAChR) in *THD'* neurons (*THD';TubGAL80^{ts} > dsmAChR*) at the indicated stages of pupal development and in adults.

Box plot symbols are as described in methods , n ≥ 30, ***p< 0.005 **p< 0.05 , n.s., not significant at p < 0.05 by one-way ANOVA followed by post hoc Tukey's test (for A and D) and n ≥ 23, ***p< 0.005 , n.s., not significant at p < 0.05 by two-tailed Student's t test (for B). All comparisons for significance were with the control values for A and C, with *itpr* mutants for B.

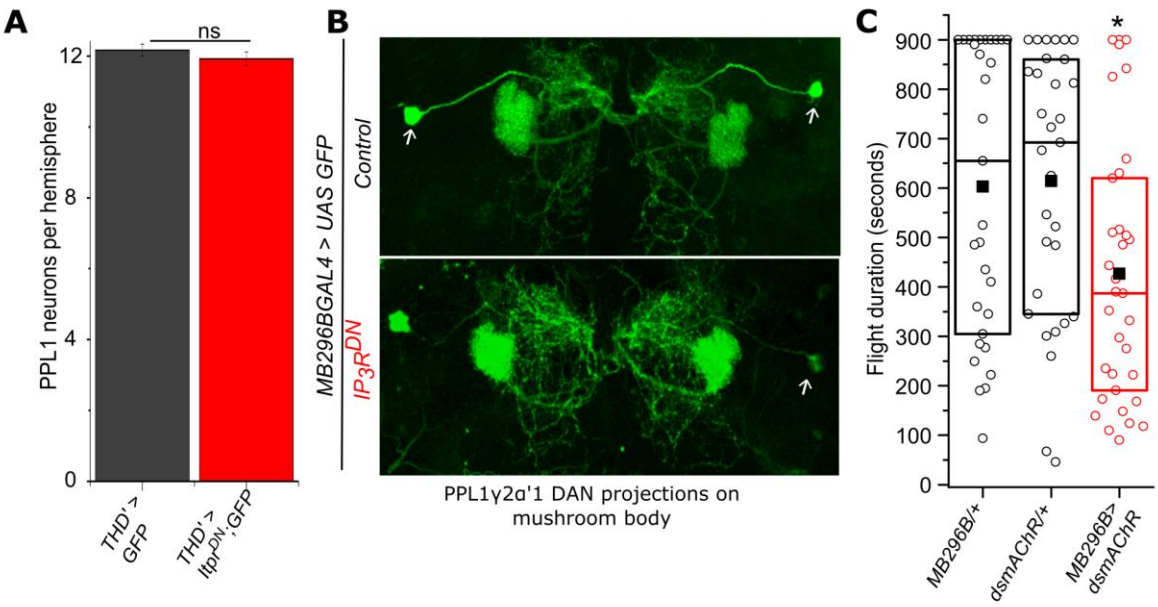

Figure 3 - figure supplement 1: Expression of IP_3R^{DN} and mAChR RNAi in *THD'* and *MB296B* marked neurons

A) Expression of IP_3R^{DN} does not change the number of PPL1 neurons. Cells were quantified from both hemi-segments of N=6 brains.

B) PPL1- γ2α'1 neurons marked by *MB296BGAL4* are shown (white arrows) with their pattern of innervation to the MB neuropil as visualized using membrane-localized GFP. Expression of IP_3R^{DN} (lower panel) did not affect the pattern of MB innervation.

C) Box plots of flight bout durations in control flies and flies with knockdown of mAChR in *MB296B* cells. $n \geq 30$, *$p < 0.05$ at $p < 0.05$ by one-way ANOVA followed by post hoc Tukey's test

314 **Synaptic vesicle release and IP_3R are both required for the function of *PPL1-γ2α'1* DANs**

315 The 48-96 hr time window of pupal development is when adult neural circuits begin
316 to mature with the formation of synapses, some of which are eliminated whilst others are
317 strengthened (Akin et al., 2019; Consoulas et al., 2002; K. X. Zhang et al., 2016). Synapse
318 strengthening occurs when pre-synaptic neurotransmitter release leads to post-synaptic
319 excitation/inhibition (Andreae & Burrone, 2018; Baines, 2003; Baines et al., 2001; Pang et al.,
320 2010) . We hypothesized that IP_3-mediated Ca^{2+} release might modulate synaptic activity
321 and hence lead to strengthening of synapses between *THD'* DANs and their post-synaptic
322 partners during pupal development. To test this idea, the requirement for synaptic vesicle
323 recycling in *THD'* and *PPL1-γ2α'1* DANs was investigated through pupal development. A
324 transgene encoding a temperature sensitive mutant of Dynamin, *Shibire^{ts}* (Vicario et al.,
325 2001), that prevents synaptic vesicle recycling at 29°C and hence blocks neurotransmitter
326 release, was expressed during pupal development, by transfer to 29°C at the appropriate
327 time interval. Loss of synaptic vesicle recycling in pupae resulted in significantly shorter flight
328 bout durations of 419.9±50.2s (*THD'*) and 411.5±57s (*MB296B*) as compared to controls
329 (Figure 4A and Figure 4 - figure supplement 1A). The requirement for synaptic vesicle
330 release was further restricted to 48-96 hrs APF consistent with the requirement of IP_3R at
331 the same time interval (Figure 3A,B). These data suggest that *THD'* marked dopaminergic
332 neurons require both synaptic vesicle recycling and IP_3-mediated Ca^{2+} release during late
333 pupal development for their adult function.

334 The acute requirement for synaptic vesicle recycling in adult PPL1 (*THD'*) and *PPL1-*
335 *γ2α'1* subset (*MB296B*) of DANs for maintenance of flight bouts was tested next. A previous
336 report shows that synaptic vesicle recycling is required in PPL1 DANs marked by *THD1GAL4*
337 during active flight (Ravi et al., 2018). We tested if synaptic vesicle release is also required in
338 *THD'* and *MB296B* marked PPL1 DANs in adults. Importantly, flight bout durations were
339 reduced significantly after acute inactivation (5 min) of synaptic vesicle recycling in PPL1
340 DANs (*THD'*) and the pair of *PPL1-γ2α'1* subset (*MB296B*) DANs in adults, supporting a
341 requirement for neurotransmitter release from these neurons during flight (Figure 4A).

342 Impaired synaptic vesicle release from adult *PPL1-γ2α'1 DANs,* by expression of
343 Shibire^{ts}, also reduces the ability of starved flies to identify a food source rapidly (Tsao et al.,
344 2018). To undertand if the IP_3R affects the function of *PPL1-γ2α'1* DANs in more than one
345 behavioural context, we tested food seeking behaviour of starved flies expressing *Itpr^{DN}* in
346 PPL1 (*THD'*) and *PPL1-γ2α'1* subset (*MB296B*) *DANs.* The food seeking index of hungry flies
347 with IP_3R^{DN} was reduced significantly as compared to controls (Figure 4B, 4C, Figure 4- figure
348 supplement 2 and Figure 4- figure supplement 3). Food-seeking behaviour of fed flies of all
349 genotypes tested appeared similar (Figure 4- figure supplement 1B).

350 Next we tested if knockdown of the mAChR, the identified flight regulating GPCR
351 (Figure 3 and Figure 3 - figure supplement 1C) that couples to IP_3/Ca^{2+} signaling, also
352 affected food seeking in starved flies. Knockdown of mAChR in either PPL1 (*THD'*) or *PPL1-*
353 *γ2α'1* decreased the ability of starved males to find a yeast drop (Figure 4D), while fed flies
354 were similar to genetic controls (Figure 4 - figure supplement 1C). Thus cholinergic

355 stimulation of IP_3/Ca^{2+} in *PPL1-γ2α′1* DANs reduces the motivation for longer flight bouts as
356 well as the motivation to search for food.
357 Taken together these data demonstrate a requirement for both synaptic vesicle
358 recycling and IP_3-mediated Ca^{2+} release in the modulation of behaviour by *PPL1-γ2α′1* DANs.
359 Furthermore, they suggest that the IP_3R might regulate synaptic function in *PPL1-γ2α′1*
360 DANs.

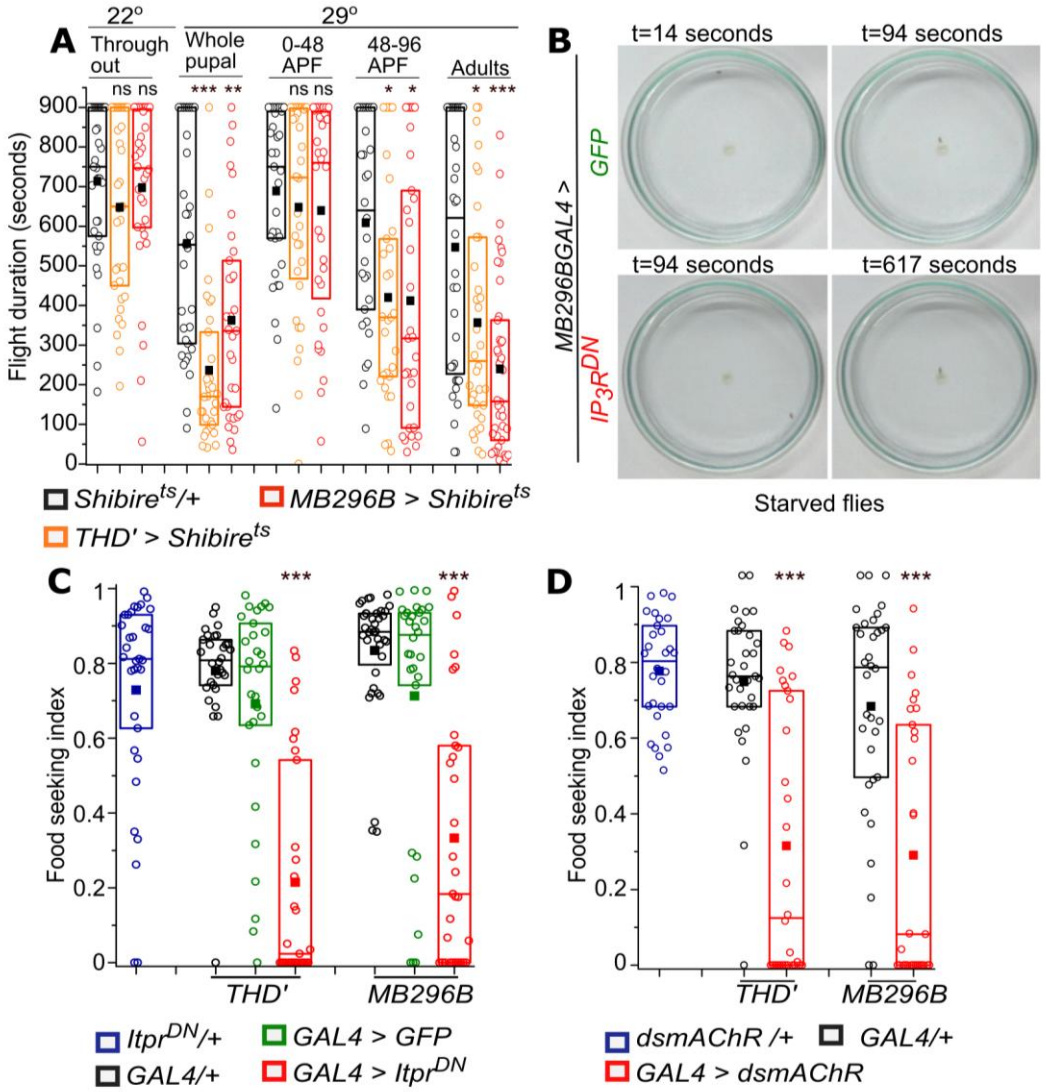

Figure 4: Synaptic vesicle recycling and IP_3R function are required in PPL1 dopaminergic neurons for adult flight and feeding

A) Quantification of flight deficits observed upon blocking synaptic vesicle recycling by expression of a temperature sensitive Dynamin mutant, *Shibire*^{ts} in *THD'* and *MB296B* cells. Inactivation of Dynamin was achieved in strains expressing *Shibire*^{ts}, by transfer to 29˚C, at the indicated stages of development. For adults, flies were grown at 22˚C and transferred to 29˚C 10 minutes before the flight assay also performed at 29˚C. n ≥ 30, ***p< 0.005, **p< 0.01, *p< 0.05 at p < 0.05 by one-way ANOVA followed by post hoc Tukey's test.

B) Food seeking by hungry flies is significantly diminished upon expression of IP_3R^{DN} in PPL1- γ2α'1 DANs (*MB296B*). Snapshots at the indicated time points from videos of starved male flies of the indicated genotype seeking a drop of yeast placed in the centre of a petriplate

C) Quantification of food seeking behavior in starved males of the indicated genotypes. Expression of IP_3R^{DN} in *THD'* and *MB296B* cells reduced food seeking behavior to a significant extent (red). Expression of *GFP* did not affect the behavior (green). n ≥ 30, ***p< 0.005 at p < 0.05 by two tailed Mann-whitney U test.

D) Quantification of food seeking behavior in starved males of the indicated genotypes. Knockdown of mAChR in *THD'* and *MB296B* cells reduced food seeking behavior to a significant extent (red, n ≥ 30, ***p< 0.005 at p < 0.05 by two tailed Mann-Whitney U test).

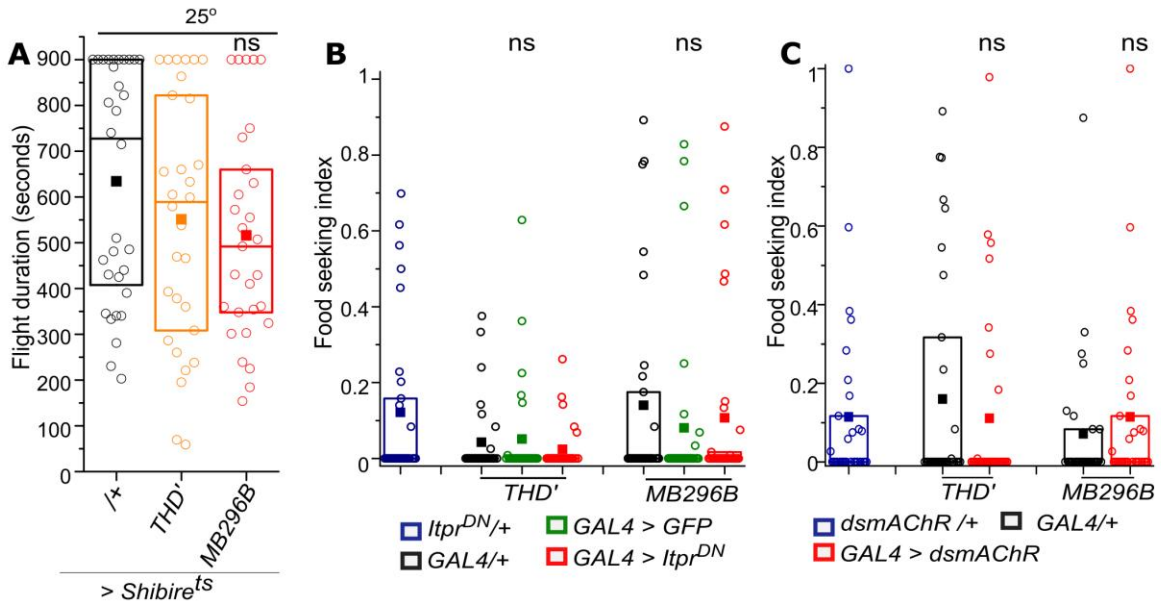

Figure 4 - figure supplement 1: Flight is unaffected and food seeking behaviour is normal in control genotypes and conditions.

A) Quantification of flight bouts upon expressing temperature sensitive dynamin mutant *Shibire*^{ts} in *THD'* and *MB296B* cells when flies were grown at the permissive temperature of 25˚C. n ≥ 30, n.s., not significant at $p < 0.05$ by one-way ANOVA followed by post hoc Tukey's test

B) Food seeking behavior is absent in fed flies including the indicated control strains and upon expression of IP_3R^{DN} in *THD'* and *MB296B* cells (red). n ≥ 30, n.s., not significant at $p < 0.05$ by two tailed Mann-whitney U test.

C) Food seeking behavior is absent in fed flies including the indicated control strains and upon knockdown of mAChR in *THD'* and *MB296B* cells (red). n ≥ 30, n.s., not significant at $p < 0.05$ by two tailed Mann-Whitney U test.

Figure 4 - figure supplement 2: Video showing food seeking behavior in control fly (*MB296BGAL4/+*)

Figure 4 - figure supplement 3: Video showing defect in food seeking behavior upon expression of IP_3R^{DN} in *MB296B* cells.

395 **The IP_3R affects neurotransmitter release from adult dopaminergic neurons:**

396 Decreased synaptic activity upon IP_3R^{DN} expression might be a consequence of a
397 reduction in synapse number. Therefore, a pre-synaptic marker, synaptotagmin tagged to
398 GFP (*syt.eGFP;* Y. Q. Zhang et al., 2002), that localises to synaptic vesicles was expressed in
399 *THD'* marked neurons in the absence and presence of IP_3R^{DN}. Fluorescence of syt.eGFP in
400 the MB lobes was no different between control brains and in presence of the IP_3R^{DN} (Figure
401 5A), suggesting that synapse numbers were unchanged by expression of IP_3R^{DN} .

402 Neurotransmitter release from *PPL1-γ2α'1* (*MB296B*) DANs in response to
403 stimulation of the IP_3R was investigated next. Presence of the mAChR was confirmed on
404 *PPL1-γ2α'1* DANs in adults by measuring Ca^{2+} release upon stimulation with the mAChR
405 agonist Carbachol. Changes in GCaMP6m fluorescence in *MB296B* marked neurons post-
406 Carbachol stimulation are shown in Figure 5 - figure supplement 1A. The ability of Carbachol
407 to stimulate dopamine release from *MB296B* marked neurons in the *γ2α'1* MB-lobe was
408 measured next. For this purpose a recently designed fluorescent sensor for dopamine,
409 $GRAB_{DA}$ (G protein-coupled receptor-activation based DA sensor; Sun et al., 2018) was
410 expressed in *MB296B* neurons followed by stimulation with Carbachol. $GRAB_{DA}$ consists of a
411 dopamine receptor linked to cpEGFP such that its fluorescence increases upon binding of
412 dopamine. Thus, a qualitative measure of dopamine release at the synaptic cleft is the
413 change in $GRAB_{DA}$ fluorescence when recorded in the *γ2α'1* MB lobe, the site of *PPL1-γ2α'1*
414 synapses (Figure 5B). Control brains, with detectable changes in $GRAB_{DA}$ fluorescence ($\Delta F/F$)
415 above an arbitrary value of 0.05 within 140 seconds of Carbachol stimulation, were classified
416 as responders. Responding brains decreased from 77% (10/13 brains) in controls to 47%
417 (8/17 brains) upon expression of IP_3R^{DN}. Moreover, $GRAB_{DA}$ fluorescence arising from
418 dopamine release was significantly muted amongst responders expressing the IP_3R^{DN} as
419 compared to responders from control brains (Figure 5B and Figure 5- figure Supplement 1B).
420 Thus expression of IP_3R^{DN} in *MB296B* DANs reduced the synaptic release of dopamine at the
421 *γ2α'1* lobe. Interestingly, increase in $GRAB_{DA}$ fluorescence at the synaptic terminals in the
422 MB was faster (Figure 5C) than the carbachol-stimulated change in GCaMP fluorescence
423 measured in the cell body (Figure 5- figure Supplement 1A). Perhaps there exist a greater
424 number of mAChRs at the synapse than on the soma of *MB296B* DANs,as mAChRs are shown
425 to be present on Kenyon cells and mushroom body (Kondo et al., 2020). Though,
426 requirement for the IP_3R and the mAChR was restricted to 48-96 hrs APF, these data suggest
427 that the neurotransmitter acetylcholine stimulates dopamine release in adult DANs through
428 mAChR-IP_3R signaling. The lack of flight deficits by adult-specific expression of IP_3R^{DN} (Figure
429 3A) and knockdown of mAChR (Figure 3C) is probably due to perdurance of the respective
430 proteins from late pupae through to adults.

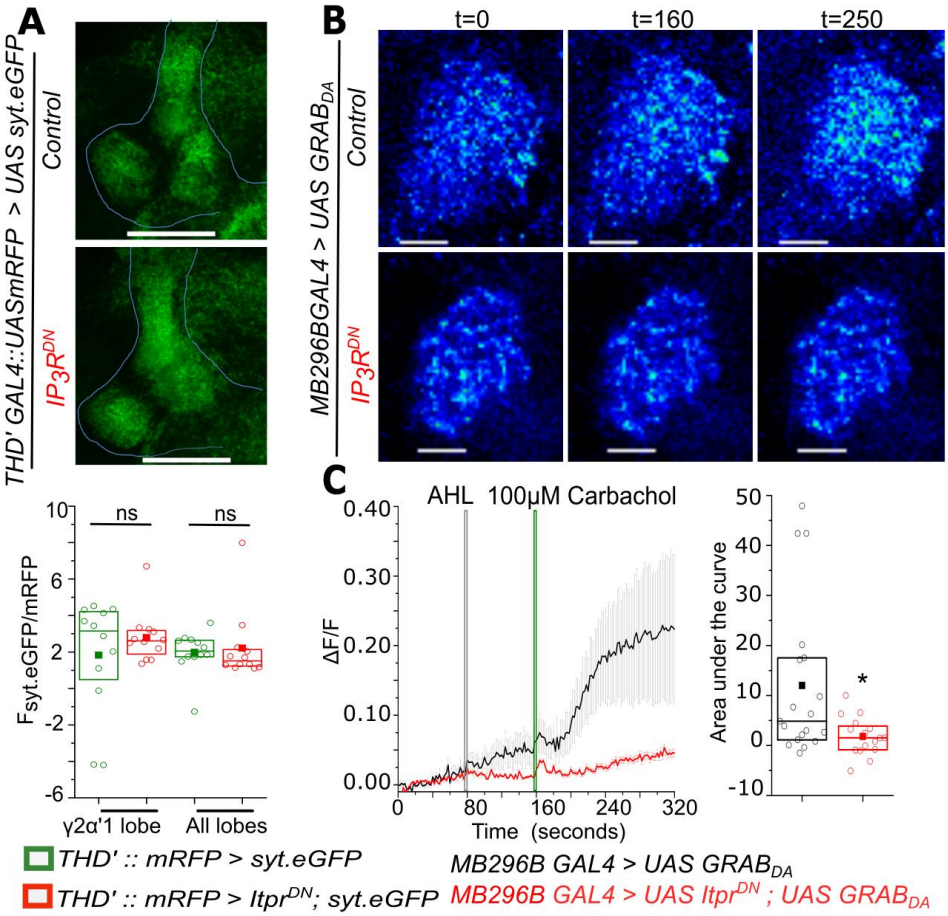

Figure 5: Carbachol-stimulated Dopamine release at the axonal terminals of *PPL1-γ2α'1* neurons is attenuated by expression of IP_3R^{DN}

A) Representative images of a presynaptic marker synaptotagmin GFP (syt.eGFP) in lobes of the Mushroom body (top). Quantification of syt.eGFP fluorescence normalized to mRFP is shown below in the indicated MB regions marked by *THD'GAL4*. N = 6 brains, n.s. not significant, by Mann Whitney U test . Scale bars indicate 50 µm

B) Carbachol stimulated dopamine release at PPL1- γ2α'1 termini visualized by changes in $GRAB_{DA}$ fluorescence in a representative mushroom body lobe from brains of the indicated genotypes. Images were acquired at 2s per frame. Brighter fluorescence denotes increase in Dopamine. Scale bars = 10 µm

C) Average traces (± SEM) of normalized $GRAB_{DA}$ fluorescence responses (ΔF/F) upon addition of Carbachol (Green line) (panel on the left); Quantification of area under the curve was from the point of stimulation at 160s and up to 250 s. Boxplots and symbols are as described in Figure 2A. *MB296B GAL4 > UAS* $GRAB_{DA}$ N = 10 brains,19 cells; *MB296B GAL4 > UAS* $Itpr^{DN}$*; UAS* $GRAB_{DA}$ N = 8 brains,16 cells. *p< 0.05, Mann-Whitney U test.

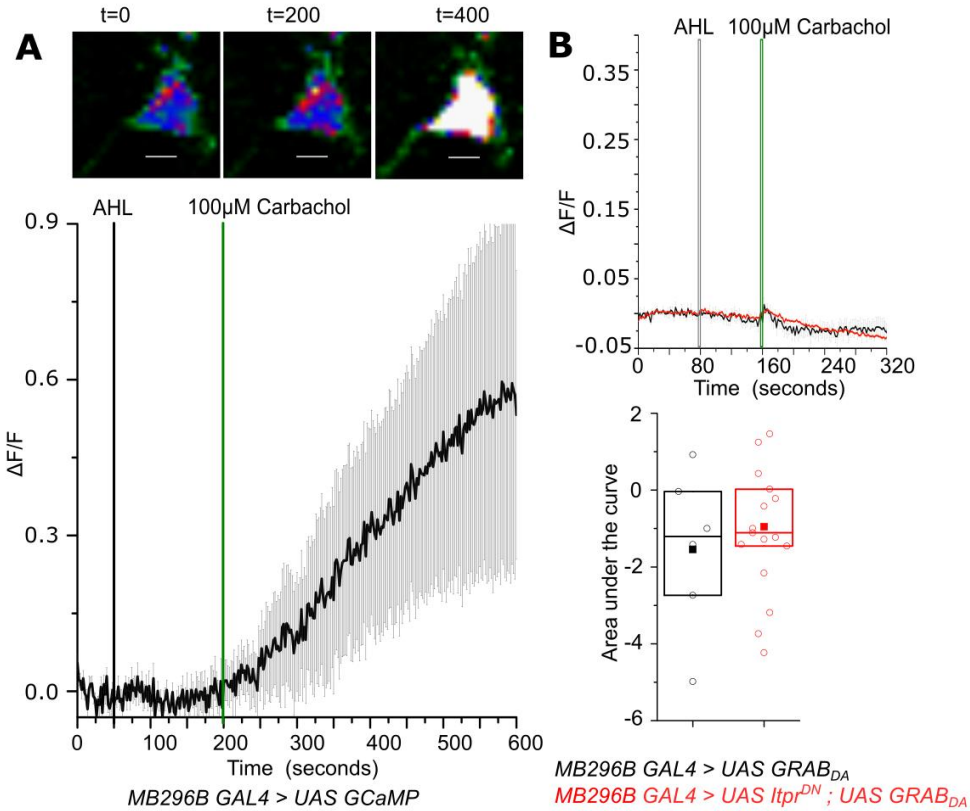

Figure 5 - figure supplement 1: Carbachol evoked Ca^{2+} responses in the soma of PPL1- γ2α'1 DANs marked by *MB296BGAL4*

A) Carbachol stimulated change in GCaMP6m fluorescence (ΔF/F) in PPL1- γ2α'1 cells. Representative images of GCaMP6m fluorescence at the indicated time points (top panel). Warmer colors denote increase in [Ca^{2+}]. Average response (± SEM) of normalized changes in GCaMP6m fluorescence (ΔF/F) in *MB296BGAL4* marked PPL1 cells upon addition of Carbachol from N=7 brains, 12 cells.

B) Average traces (± SEM) of normalized changes in $GRAB_{DA}$ fluorescence (ΔF/F) from axonal termini of *MB296B*GAL4 marked DANs that responded below the arbitrary threshold (ΔF/F=0.05) upon addition of Carbachol (Green line) (Top panel). Quantification of area under the curve (AUC) from the point of stimulation 160s up to 250s. Boxplots and symbols are as described in Figure 2A. *MB296B GAL4 > UAS GRAB$_{DA}$* N = 3 brains, 6 cells; *MB296B GAL4 > UAS Itpr^{DN}; UAS GRAB$_{DA}$* N = 9 brains, 17 cells *p< 0.05, Mann Whitney U test. (lower panel).

460 **The IP_3R helps maintain membrane excitability of *PPL1-γ2α'1* neurons**

461 In addition to the neuromodulatory input of acetylcholine, the *PPL1-γ2α'1* DANs are
462 likely to receive direct excitatory inputs. Therefore next we investigated if loss of IP_3/Ca^{2+}
463 signals alter the essential properties of neuronal excitability of *MB296B* neurons. Stimulation
464 by activation of an optogenetic tool, *CsChrimson* (Klapoetke et al., 2014) was followed by
465 measuring changes in fluorescence of the Ca^{2+} sensor GCaMP in ex-vivo brain preparation. In
466 neurons expressing IP_3R^{DN} and GCaMP optogenetic stimulation of CsChrimsom did not evince
467 a significant Ca^{2+} response as compared with the control genotype expressing RFP and
468 GCaMP (Figure 6A, B). Similar results were obtained by KCl-evoked depolarisation in the
469 presence of 2 µM Tetrodotoxin (TTX) (Figure 6- figure supplement 1A, B). TTX was added so
470 as to prevent excitation by synaptic inputs from other neurons upon KCl addition. These data
471 suggest that neurons with IP_3R^{DN} fail to respond to a depolarising stimulus. This idea was
472 tested directly by measuring the change in membrane potential in response to
473 depolarisation, with a genetically encoded fluorescent voltage indicator, *Arclight* (Cao et al.,
474 2013). There was an instant decline in Arclight fluorescence in control cells, while cells with
475 IP_3R^{DN} showed almost no change in fluorescence after KCl mediated depolarisation (Figure
476 6C, D). Taken together, these observations confirm that signaling through the IP_3R is also
477 required for maintaining excitability of central neuromodulatory dopaminergic neurons.

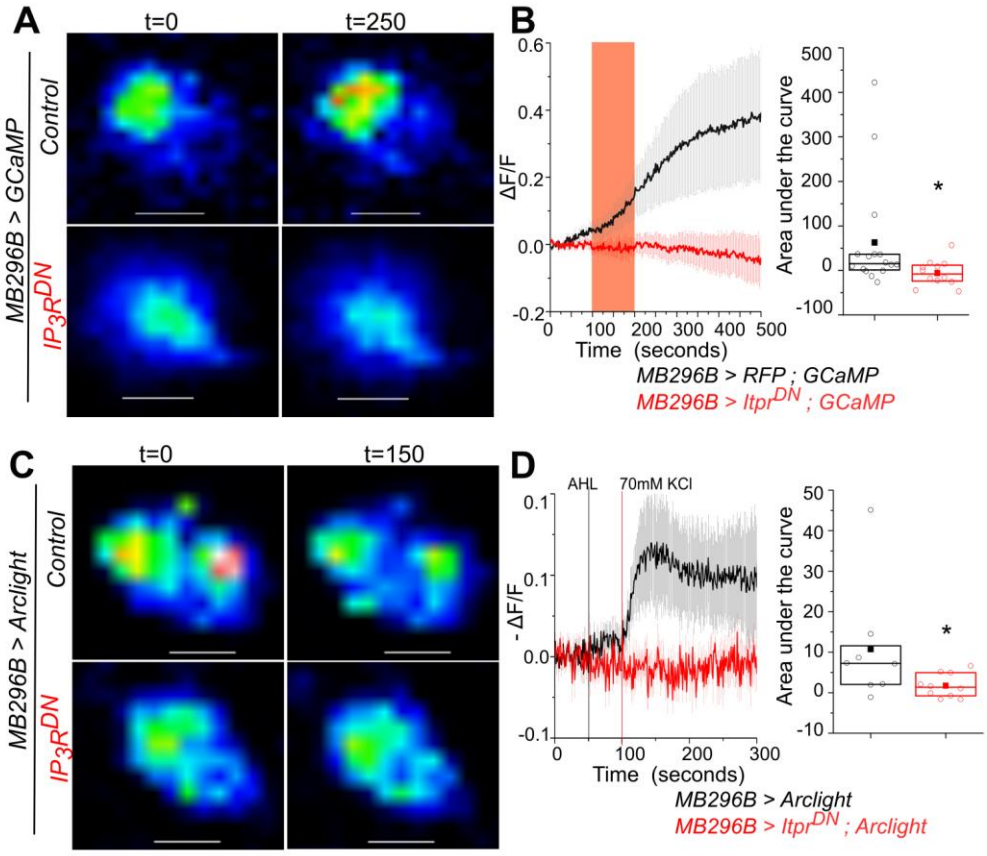

Figure 6: Optimal excitability of PPL1- γ2α′1 dopaminergic neurons requires the IP_3R

A) Optogenetic activation of PPL1- γ2α′1 DANs, with the red light activated Channelrhodopsin variant Chrimson, is attenuated by expression of IP_3R^{DN}. Representative images of *MB296BGAL4* marked DANs of the indicated genotypes are shown with changes in GCaMP6m fluorescence before (t=0) and after t=250s a 100s pulse of red light (red bar). Images were acquired at 2s per frame. Warmer colors denote increase in $[Ca^{2+}]$. Scale bar = 5 µm (Top).

B) Average traces (± SEM) of normalized changes in GCaMP6m fluorescence (ΔF/F) in *MB296BGAL4* marked DANs after activation by Chrimson (left); Quantification of area under the curve from the point of stimulation at 100s up to 400 s. Boxplots and symbols are as described in Figure 2A. *MB296B GAL4 > UAS RFP; UAS GCaMP* N = 7 brains 20 cells; *MB296B GAL4 > UAS Itpr^{DN}; UAS GCaMP* N = 7 brains, 10 cells *p< 0.05 , Mann whitney U test. (right).

C) Changes in membrane potential upon addition of KCl, visualized by expression of the voltage sensor Arclight. Representative images of Arclight responses in *MB296BGAL4* marked DANs are shown from the indicated genotypes and time points. Images were acquired at 1s per frame; Scale bar = 5 µm (Top).

D) Average traces (± SEM) of normalized changes in Arclight fluorescence (ΔF/F) in *MB296BGAL4* marked DANs after addition of KCl (left); Quantification of area under the curve from the point of stimulation at 100s up to 200 s. Boxplots and symbols are as described in Figure 2A. *MB296B GAL4 > UAS Arclight* N = 7 brains 8 cells; *MB296B GAL4 > UAS Itpr^{DN}; UAS Arclight* N = 8 brains, 10 cells *p< 0.05 , Mann Whitney U test. (right).

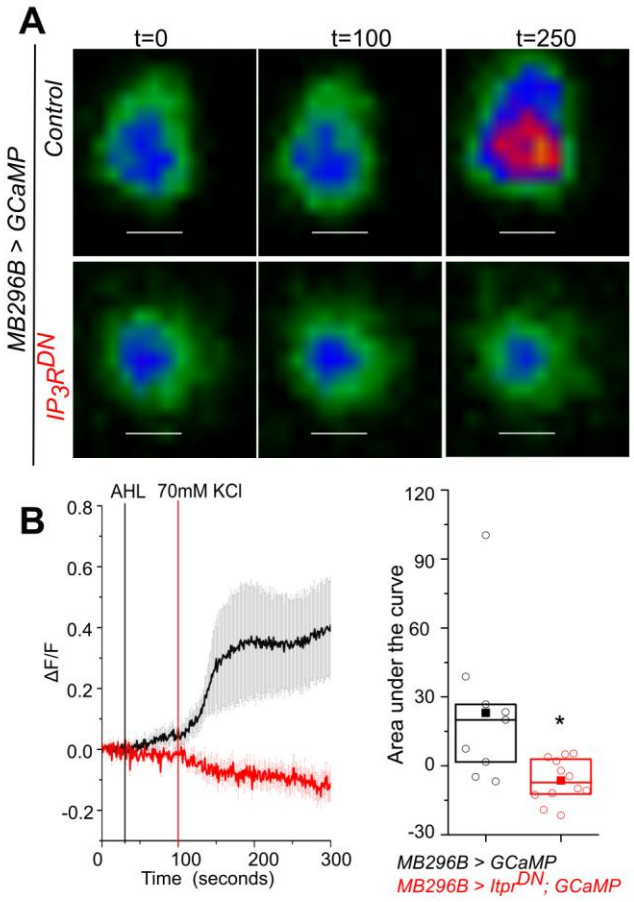

Figure 6 - figure supplement 1: Perturbation of IP_3R signaling in PPL1- γ2α′1 cells reduced KCl evoked calcium response:

A) KCl evoked activation of PPL1- γ2α′1 DANs is attenuated by expression of IP_3R^{DN}. Representative images of *MB296BGAL4* marked DANs of the indicated genotypes are shown with changes in GCaMP6m fluorescence before (t=0, t=100) and after addition of KCl at t=250s. Images were acquired at 1s per frame. Warmer colors denote increase in $[Ca^{2+}]$. Scale bar = 5 µm (Top).)

B) Average traces (± SEM) of normalized changes in GCaMP6m fluorescence (ΔF/F) in *MB296BGAL4* marked DANs after activation by KCl (left); Quantification of area under the curve from the point of stimulation at 100s up to 200 s. Boxplots and symbols are as described in Figure 2A. *MB296B GAL4 > UAS GCaMP* N = 5 brains, 9 cells; *MB296B GAL4 > UAS Itpr^{DN}; UAS GCaMP* N = 6 brains, 12 cells *p< 0.05 , Mann whitney U test (right).

511 **Discussion:**

512 An inducible IP_3R^{DN} construct developed and used in this study allowed us to perform
513 stage and cell specific attenuation of IP_3R mediated calcium signaling *in vivo*. Consistent with
514 well characterised phenotypes of IP_3R mutants (Banerjee et al., 2004), neuronal expression
515 of IP_3R^{DN} affected flight. Spatiotemporal studies identified a requirement for the IP_3R in a
516 small subset of central dopaminergic neurons for maintenance of adult flight bouts as well as
517 in the food-seeking behaviour of hungry flies. Inhibition of synaptic release in the identified
518 dopaminergic subset also reduced the duration of flight bouts. Dopamine release at
519 synapses in the MB γ2α'1 lobe was significantly attenuated in adults expressing the IP_3R^{DN}
520 (carried over from late pupae). These animals in addition exhibit reduced membrane
521 excitability. Intracellular Ca^{2+} signaling through the IP_3R is thus required to ensure optimal
522 neuronal excitability and synaptic function in specific central dopaminergic neurons that
523 appear to drive the motivation for both longer flight bouts and the search for food in a
524 hungry fly (Figure 7).

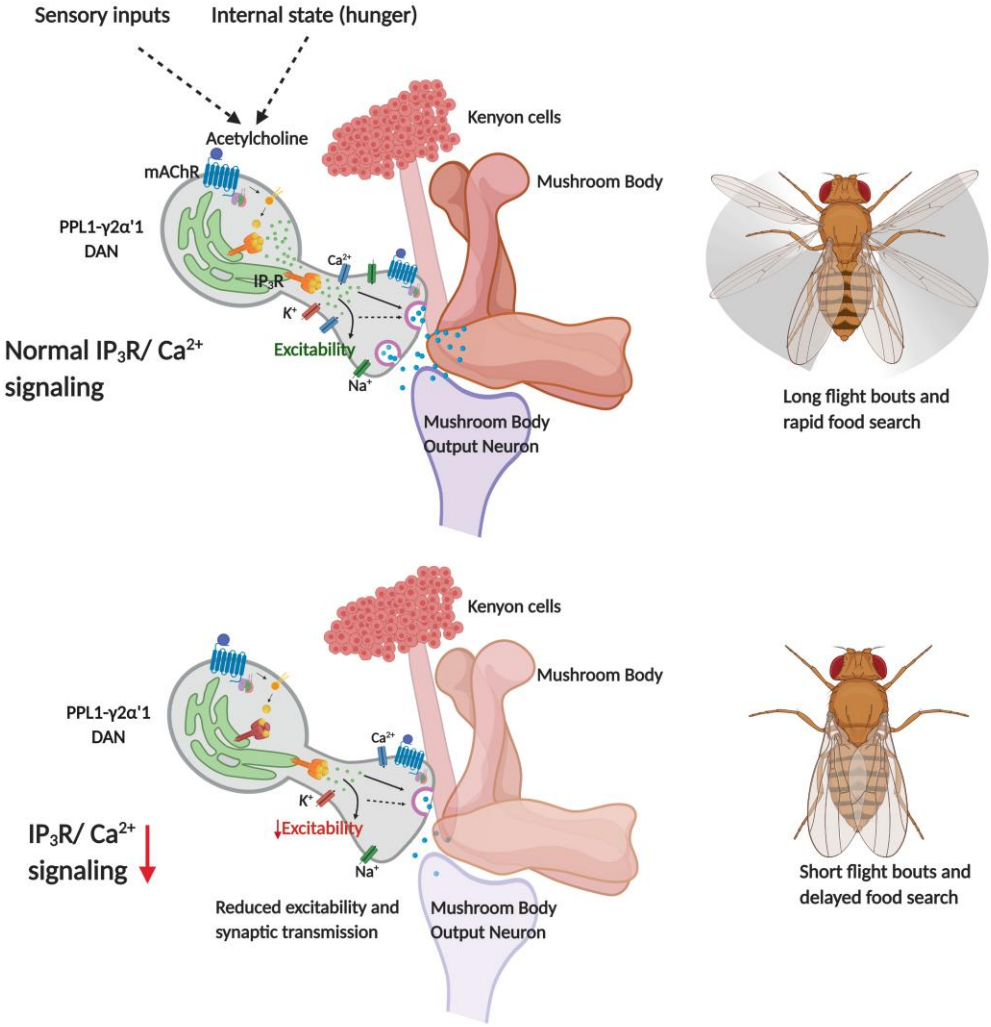

Figure 7: Schematic showing neuronal properties regulated by IP_3/Ca^{2+} signals in central dopaminergic neurons for flight and food search behaviour in *Drosophila melanogaster*

528 **The IP_3R and synaptic release in pupae and adults**

529 Temporal expression of IP_3R^{DN} demonstrated a requirement during circuit maturation
530 in late pupae but not in adults. However, these data do not rule out an acute function for the
531 IP_3R in adult dopaminergic neurons because functional wild-type tetramers of the IP_3R
532 assembled during pupal development very likely mask the effect of adult specific expression
533 of IP_3R^{DN}. Taken together with the short flight bouts observed upon expression of *Shibire*^{ts}
534 either in late pupae or in adults, our data support a model where mAChR stimulated ER-Ca^{2+}
535 signals through the IP_3R regulate synaptic release of dopamine from PPL1- γ2α'1 DANs
536 during circuit maturation and during adult flight. Both direct and indirect effects of ER-Ca^{2+}
537 on synaptic vesicle release have been observed in vertebrates (Gomez et al., 2020; Rossi et
538 al., 2008; Sharma & Vijayaraghavan, 2003) and *Drosophila* (James et al., 2019; Klose et al.,
539 2010; Richhariya et al., 2018; Shakiryanova et al., 2011). Further studies are required to
540 identify the molecular mechanism by which ER-Ca^{2+} signals regulate dopamine release in
541 PPL1- γ2α'1 DANs.

542 **Intracellular Ca^{2+} signaling and neuronal excitability**

543 Genetic manipulations that target intracellular calcium signaling are known to affect
544 the intrinsic excitability of neurons. For example Purkinje neurons in mice with cell-specific
545 knockout of the ER-Ca^{2+} sensor Stim1, that functions downstream of mGluR1, exhibit a
546 decreased frequency of firing (Ryu et al., 2017). In *Drosophila* FMRFa Receptor mediated
547 calcium signaling modulates the excitability of PPL1 dopaminergic neurons through CAMKII
548 (Ravi et al., 2018). Reduced excitability of dopaminergic neurons expressing the IP_3R^{DN}
549 transgene (Figure 6 and Figure 6- figure supplement 1) further supports a role for
550 intracellular calcium signals in setting the threshold of membrane excitability in response to
551 neuromodulatory signals, such as acetylcholine (this study), the FMRFa neuropeptide (Ravi
552 et al., 2018) and glutamate (Ryu et al., 2017).

553 The cellular mechanism(s) by which IP_3/Ca^{2+} signals regulate neuronal excitability
554 probably vary among different classes of neurons. In addition to the direct activation of Ca^{2+}
555 dependant enzymes such as CamKII, previous reports have shown that knock-down of the
556 IP_3R in *Drosophila* larval neurons alters their expression profile and specifically affects the
557 expression of several membrane localised ion-channels (Jayakumar et al., 2018). Reduced
558 translation of proteins due to IP_3R knockdown has also been demonstrated in peptidergic
559 neurons (Megha & Hasan, 2017). Changes in membrane excitability could thus derive from
560 direct regulation of ion channels by Ca^{2+} and Ca^{2+} dependant enzymes as well as an altered
561 density of specific ion channels. Moreover, Ca^{2+} release through the IP_3R regulates
562 mitochondrial Ca^{2+} entry (Figure 1E). Expression of IP_3R^{DN} might thus impact neuronal firing
563 and synaptic release by changes in cellular bioenergetics (Cárdenas et al., 2010; Chouhan et
564 al., 2012) .

565 **PPL1- γ2α'1 DANs, flight and the search for food**

A role for the PPL1 cluster of dopaminergic neurons in modulating flight and longer flight bouts has been reported earlier (Pathak et al., 2015; Ravi et al., 2018). However, amongst the PPL1 cluster this is the first report identifying the two PPL1- γ2α′1 DANs as required for maintenance of flight. The PPL1- γ2α′1 DANs and their downstream Mushroom body output neuron (MBON- γ2α′1) also encode the state of hunger (Tsao et al., 2018), formation and consolidation of appetitive memory (Berry et al., 2018; Felsenberg et al., 2017; Yamazaki et al., 2018) and sleep (Aso et al., 2014; Sitaraman et al., 2015). These studies identified the importance of modulated dopamine release as a motivational cue wherein dopamine release from PPL1- γ2α′1 DANs increased in starved flies (Tsao et al., 2018) and inhibited the activity of a cholinergic output neuron from the Mushroom Body (MBON- γ2α′1; Tsao et al., 2018). The MBON- γ2α′1 projects to another set of central DANs, the PAM neurons (Felsenberg et al 2017), identified as flight promoting in a previous study (Manjila et al., 2019). This leads to the hypothesis that inputs to the PPL1- γ2α′1 DANs through mAChR driven IP_3/Ca^{2+} signals modulate dopamine release at the PPL1- γ2α′1> MBON- γ2α′1 synapse, and the extent of dopamine release changes the output strength of MBON- γ2α′1. Altered MBON- γ2α′1 outputs might then regulate flight through the PAM-DANs and their downstream circuits. Prolonged flight bouts are energy intensive and very likely require multisensory integration for their continuation. Modulated activity in the PPL1-γ2α′1 DANs forms an important component of this integration and can lead to inhibition of MBON- γ2α′1 so as to maintain wakefulness (Aso et al., 2014; Sitaraman et al., 2015) as well as increase the search for food when hungry (Tsao et al., 2018). The integration of external cues that stimulate flight with the internal states of hunger and wakefulness very likely serve important functions of survival in the wild.

589 **Materials and methods:**

590 **Fly stocks:** *Drosophila* strains used in this study were reared on cornmeal media,
591 supplemented with yeast. Flies were maintained at 25˚C, unless otherwise mentioned under
592 12:12 light: dark cycle. WT strain of *Drosophila* used was *Canton S*.

593 Following fly lines were kindly provided by various fly community members across the globe
594 as mentioned: *THGAL4* (Friggi-Grelin et al., 2003) by Serge Birman (CNRS, ESPCI Paris Tech,
595 France), *THD'* GAL4 (Liu et al., 2012) from Mark N Wu (Johns Hopkins University, Baltimore),
596 *UAS* $GRAB_{DA}$ (Sun et al., 2018) from Youlong Li (Peking University School of Life Sciences,
597 Beijing, China), *UAS* $Shibire^{ts}$ (Vicario et al., 2001) from Toshihiro Kitamoto (University of
598 Iowa, Carver College of Medicine, Iowa). $vGlut^{VGN6341}GAL4$ (Syed et al., 2016) from K.
599 Vijayraghavan (NCBS, India), *UAS mitoGCaMP* (Lutas et al., 2012) from Fumiko Kawasaki
600 (Pennsylvania State University, Pennsylvania). A strain with two copies of $TubGAL80^{ts}$ on the
601 third chromosome was generated by Albert Chiang, NCBS, Bangalore, India, and has been
602 used for all $Gal80^{ts}$ experiments. Single-point mutants of the *itpr* gene ($Itpr^{ka1091}$, $itpr^{ug3}$)
603 were characterized as described previously (Joshi et al., 2004)

604 The fly lines *nSybGAL4* (BL51635), *UAS GCaMP6m* (BL42748), *UAS Arclight* (BL51057),
605 *UASmCD8GFP* (BL5130), *UAS Dicer* (BL24648), *UAS Chrimson* (BL55136), *UAS syt.eGFP*
606 (BL6926), *MB058BGAL4* (BL68278), *MB296BGAL4* (BL63308), *MB304BGAL4* (BL68367),
607 *MB320CGAL4* (BL68253), *MB630BGAL4* (BL68334), *MB438BGAL4* (BL68326), *MB504BGAL4*
608 (BL68329) were obtained from Bloomington Drosophila Stock Centre (BDSC). The *UAS*
609 *itprRNAi* (1063-R2) strain was from National Institute of Genetics (NIG), *UAS mAChR RNAi*
610 was from VDRC (101407)

611 **Single flight assay:** Flight assays were performed according to Manjila & Hasan, 2018. Briefly,
612 3-5 day old flies of either sex were tested in batches of 8-10 flies. They were anaesthesized
613 on ice for 2-3 minutes and then tethered between their head and thorax using a thin metal
614 wire and nail polish. Once recovered, mouth blown air puff was given as a stimulus to initiate
615 flight and flight time was recorded for each fly till 15 minutes. For all control genotypes,
616 *GAL4* or *UAS* strains were crossed to wild type strain, *Canton S.* Flight time data is
617 represented in the form of boxplots using Origin software (OriginLab, Northampton, MA).
618 Each box represents 25th to 75th percentile, each open circle represents flight duration of a
619 single fly, solid squares represent the mean and the horizontal line in each box represents
620 the median.

621 For $Gal80^{ts}$ experiments, larvae, pupae or adults were maintained at 18˚C and transferred to
622 29˚C only at the stage when the *UAS* transgene needed to be expressed. Flight assay was
623 done at 25˚C. For adult specific expression, flies were grown at 18˚C and transferred to 29˚C
624 immediately after eclosion for 2-3 days. For experiments involving $Shibire^{ts}$, larvae, pupae or
625 adults were maintained at 22˚C and transferred to 29˚C only at the stage when the $Shibire^{ts}$
626 needs to be activated. Flight assay was done at 25˚C except for adult specific activation in

627 which flies were shifted to 29˚C ten minutes before flight assay and then maintained at 29˚C
628 during the experiment.

629 For optogenetic experiments, flies were transferred to media containing 200 mM all-trans-
630 retinal (ATR) and reared in dark for 2-3 days before imaging experiments.

631 **Ex vivo live Imaging:** Adult brains were dissected in Adult hemolymph-like (AHL) saline (108
632 mM NaCl, 5 mM KCl, 2 mM CaCl2, 8.2 mM MgCl2, 4 mM NaHCO3, 1 mM NaH2PO4, 5 mM
633 trehalose, 10 mM sucrose, 5 mM Tris, pH 7.5) while larval brains were dissected in HL3 (70
634 mm NaCl, 5 mm KCl, 20 mm MgCl2, 10 mm NaHCO3, 5 mm trehalose, 115 mm sucrose, 5
635 mm HEPES, 1.5 mm Ca2+, pH 7.2). The dissected brain was mounted on culture dish with
636 anterior side up for recording from cell while posterior side up for imaging mushroom body.
637 They were then embeded in 6µl of 1% low-melt agarose (Invitrogen), and bathed in AHL.
638 Images were taken as a time series on an XY plane using a 20x objective on an Olympus
639 FV3000 inverted confocal microscope (Olympus Corp.) . Acquisition time is different for
640 different experiments and is described in the figure legends. GCaMP6m, Arclight and $GRAB_{DA}$
641 signals were captured using the 488 nm excitation laser line while 633nm laser was used for
642 optogenetic stimulation of Chrimson.

643 Raw fluorescence data were extracted from the marked ROIs using a time series analyzer
644 plugin in Fiji (Balaji, https://imagej.nih.gov/ij/plugins/time-series.html). ΔF/F was calculated
645 using the following formula for each time point (t): $\Delta F/F = (F_t - F_0)/F_0$, where F_0 is the average
646 basal fluorescence of the first 20 frames.

647 To quantify response to stimuli we calculated area under the curve(AUC). Area under the
648 curve was calculated from the point of stimulation till mean peak response was reached
649 using Microsoft Excel (Microsoft). Time frame for calculating AUC is mentioned in figure
650 legends. AUC is represented as boxplots using Origin software (OriginLab, Northampton,
651 MA). Each box represents 25th to 75th percentile, each open circle represents flight duration
652 of a single fly, solid squares represent the mean and the horizontal line in each box
653 represents the median.

654 **Generation of IP_3R^{DN}:** Five *itpr* residues in *Drosophila itpr* cDNA (Sinha & Hasan, 1999) were
655 mutated using site directed mutagenesis kit (Agilent). The oligonucleotide
656 CAGAGATCGGCAG**C**AATTGCTGC**AG**GAACAGTACATCC was used to change K530/R533 to Q
657 while GTACCACGTCTTTCTGC**AG**ACCACCGGACGCACCAG was used to change R272 to Q. All
658 mutations were confirmed using Sanger's sequencing. Mutated *itpr* cDNA was subcloned in
659 *UAS attB* vector (Bischof et al., 2007). *UAS* $Itpr^{DN}$ plasmid was then microinjected in fly
660 embryos at the NCBS fly facility to obtain stable fly strains using standard protocols of fly
661 embryo injection .

662 **Food seeking assay:** Food seeking assay was performed according to Tsao et al., 2018.
663 Briefly, 18-20 hrs starved males (4 days old) of specified genotypes were introduced in

664 petridish (dimensions) with drop of yeast solution in the centre. The yeast solution was
665 prepared by mixing 0.2 gram of yeast with 1 gram of sugar in 5 ml distilled water and
666 incubated in a 28°C shaking incubator (170 rpm) for 16 hr. Starved males were then allowed
667 to search for food and it was considered having found food if it rested for 3 sec or longer on
668 food drop. Food-seeking index was calculated as: [Total assay time (600 s) - the time taken to
669 locate food (sec)]/Total assay time (600 s).

670 **Immunohistochemistry:** Immunohistochemistry was performed on dissected adult brains as
671 described in Pathak et al., 2015. Briefly, brains were dissected in 1x PBS, followed by fixation
672 in 4% paraformaldehyde for 30 minutes at room temperature and then 3-4 washings with
673 0.2% phosphate buffer, pH 7.2 containing 0.2% Triton-X 100 (PTX) . They were then blocked
674 in 0.2% PTX containing 5% normal goat serum for four hours at 4°C and incubated overnight
675 with primary antibodies. Next day, they were washed three to four times with 0.2% PTX at
676 room temperature, and then incubated with the respective fluorescent secondary
677 antibodies for 2 hr at room temperature. The primary antibodies used were: rabbit anti GFP
678 (1:10,000, A6455, Life Technologies), mouse anti-bruchpilot (anti-brp) antibody (1:50; kindly
679 provided by Eric Buchner, Univerity of Wuerzburg, Germany). Fluorescent secondary
680 antibodies used at were anti-mouse Alexa Fluor 568 (1:400, #A11004, Life Technologies) and
681 anti-rabbit Alexa Fluor 488 (1:400, #A11008, Life Technologies). Confocal images were
682 obtained on the Olympus Confocal FV3000 microscope (Olympus Corp.) with a 20x or with a
683 40x objective. Images were visualized using Fiji.

684 **Western Blots:** Between 5 to 10 pupal and adult brains or adult heads of appropriate
685 genotypes were dissected in cold PBS and were homogenized in 30 µl of homogenizing
686 buffer (25 mM HEPES, pH 7.4, 150 mM NaCl, 5% glycerol, 1 mM DTT, 1% Triton X-100, and 1
687 mM PMSF). 15 µl of the homogenate was run on a 5% SDS-polyacrylamide gel. The protein
688 was transferred to a nitrocellulose membrane by standard protocols. Membrane was then
689 blocked with 5% skim milk followed by incubation with primary antibody at 4°C overnight.
690 The affinity-purified anti-IP_3R rabbit polyclonal antibody (Agrawal et al., 2009) (IB-9075) was
691 used at a dilution of 1:300 and mouse anti-spectrin antibody (1:50; 3A9, DSHB) was used as a
692 loading control for IP_3R. Secondary antibodies conjugated with horseradish peroxidase were
693 used at dilution of 1:3000 (anti-mouse HRP; 7076S, Cell Signaling Technology) and 1:5000
694 (anti-rabbit HRP; 32260, Thermo Scientific). The protein was then detected on the blot by a
695 chemiluminiscent detection solution (Advansta).

696 **Statistical tests:** For flight data, two-tailed Student's t test was used to compare two samples
697 while one-way ANOVA followed by post hoc Tukey's test was used if more than two
698 conditions were involved. All statistical tests were performed using Origin 8.0 software
699 (Micro Cal). Statistical tests and p-values are mentioned in each figure legend. For food
700 seeking assay as well as imaging data, Two-tailed Mann-Whitney U test was performed to
701 statistically validate the significance.

702 Model in Figure 7 was created using Biorender (BioRender.com)

References:

Agrawal, N., Padmanabhan, N., & Hasan, G. (2009). Inositol 1,4,5- trisphosphate receptor function in Drosophila insulin producing cells. *PLoS ONE*, *4*(8), e6652. https://doi.org/10.1371/journal.pone.0006652

Akin, O., Bajar, B. T., Keles, M. F., Frye, M. A., & Zipursky, S. L. (2019). Cell-type-Specific Patterned Stimulus-Independent Neuronal Activity in the Drosophila Visual System during Synapse Formation. *Neuron*, *101*(5), 894-904 https://doi.org/10.1016/j.neuron.2019.01.008

Alzayady, K. J., Wang, L., Chandrasekhar, R., Wagner, L. E., Van Petegem, F., & Yule, D. I. (2016). Defining the stoichiometry of inositol 1,4,5-trisphosphate binding required to initiate Ca2+ release. *Science Signaling*, *9*(422), ra35-ra35. https://doi.org/10.1126/scisignal.aad6281

Ando, H., Hirose, M., & Mikoshiba, K. (2018). Aberrant IP3 receptor activities revealed by comprehensive analysis of pathological mutations causing spinocerebellar ataxia 29. *Proceedings of the National Academy of Sciences of the United States of America*, *115*(48), 12259–12264. https://doi.org/10.1073/pnas.1811129115

Andreae, L. C., & Burrone, J. (2018). The role of spontaneous neurotransmission in synapse and circuit development. In *Journal of Neuroscience Research,* 96(3), 354-359.. https://doi.org/10.1002/jnr.24154

Aso, Y., Hattori, D., Yu, Y., Johnston, R. M., Iyer, N. A., Ngo, T. T. B., Dionne, H., Abbott, L. F., Axel, R., Tanimoto, H., & Rubin, G. M. (2014). The neuronal architecture of the mushroom body provides a logic for associative learning. *eLife*, *3,* e04677. https://doi.org/10.7554/eLife.04577

Aso, Y., & Rubin, G. M. (2016). Dopaminergic neurons write and update memories with cell-type-specific rules. *eLife*, *5,* e16135. https://doi.org/10.7554/eLife.16135

Aso, Y., Sitaraman, D., Ichinose, T., Kaun, K. R., Vogt, K., Belliart-Guérin, G., Plaçais, P. Y., Robie, A. A., Yamagata, N., Schnaitmann, C., Rowell, W. J., Johnston, R. M., Ngo, T. T. B., Chen, N., Korff, W., Nitabach, M. N., Heberlein, U., Preat, T., Branson, K. M., … Rubin, G. M. (2014). Mushroom body output neurons encode valence and guide memory-based action selection in Drosophila. *eLife*, *3*, e04580. https://doi.org/10.7554/eLife.04580

Baines, R. A. (2003). Postsynaptic protein kinase A reduces neuronal excitability in response to increased synaptic excitation in the Drosophila CNS. *Journal of Neuroscience*, *23*(25), 8664-8672. https://doi.org/10.1523/jneurosci.23-25-08664.2003

Baines, R. A., Uhler, J. P., Thompson, A., Sweeney, S. T., & Bate, M. (2001). Altered Electrical Properties in Drosophila Neurons Developing without Synaptic Transmission. *The Journal of Neuroscience*, *21*(5), 1523–1531. https://doi.org/10.1523/JNEUROSCI.21-05-01523.2001

Banerjee, S., Joshi, R., Venkiteswaran, G., Agrawal, N., Srikanth, S., Alam, F., & Hasan, G. (2006). Compensation of inositol 1,4,5-trisphosphate receptor function by altering sarco-endoplasmic reticulum calcium ATPase activity in the Drosophila flight circuit.

Journal of Neuroscience, *26*(32), 8278–8288. https://doi.org/10.1523/JNEUROSCI.1231-06.2006

Banerjee, S., Lee, J., Venkatesh, K., Wu, C. F., & Hasan, G. (2004). Loss of flight and associated neuronal rhythmicity in inositol 1,4,5-trisphosphate receptor mutants of Drosophila. *Journal of Neuroscience*, *24*(36), 7869–7878. https://doi.org/10.1523/JNEUROSCI.0656-04.2004

Bartok, A., Weaver, D., Golenár, T., Nichtova, Z., Katona, M., Bánsághi, S., Alzayady, K. J., Thomas, V. K., Ando, H., Mikoshiba, K., Joseph, S. K., Yule, D. I., Csordás, G., & Hajnóczky, G. (2019). IP3 receptor isoforms differently regulate ER-mitochondrial contacts and local calcium transfer. *Nature Communications*, *10*(1), 1–14. https://doi.org/10.1038/s41467-019-11646-3

Berridge, M. J. (2016). The inositol trisphosphate/calcium signaling pathway in health and disease. *Physiological Reviews*, *96*(4), 1261–1296. https://doi.org/10.1152/physrev.00006.2016

Berry, J. A., Phan, A., & Davis, R. L. (2018). Dopamine Neurons Mediate Learning and Forgetting through Bidirectional Modulation of a Memory Trace. *Cell Reports*, *25*(3), 651-662. https://doi.org/10.1016/j.celrep.2018.09.051

Bischof, J., Maeda, R. K., Hediger, M., Karch, F., & Basler, K. (2007). An optimized transgenesis system for Drosophila using germ-line-specific ϕC31 integrases. *Proceedings of the National Academy of Sciences of the United States of America*, *104*(9), 3312-3317. https://doi.org/10.1073/pnas.0611511104

Cárdenas, C., Miller, R. A., Smith, I., Bui, T., Molgó, J., Müller, M., Vais, H., Cheung, K. H., Yang, J., Parker, I., Thompson, C. B., Birnbaum, M. J., Hallows, K. R., & Foskett, J. K. (2010). Essential Regulation of Cell Bioenergetics by Constitutive InsP3 Receptor Ca2+ Transfer to Mitochondria. *Cell*, *142*(2), 270–283. https://doi.org/10.1016/j.cell.2010.06.007

Chakraborty, S., & Hasan, G. (2012). Functional complementation of Drosophila itpr mutants by rat Itpr1. *Journal of Neurogenetics*, *26*(3–4), 328–337. https://doi.org/10.3109/01677063.2012.697501

Chen, T. W., Wardill, T. J., Sun, Y., Pulver, S. R., Renninger, S. L., Baohan, A., Schreiter, E. R., Kerr, R. A., Orger, M. B., Jayaraman, V., Looger, L. L., Svoboda, K., & Kim, D. S. (2013). Ultrasensitive fluorescent proteins for imaging neuronal activity. *Nature*, *499*(7458), 295–300. https://doi.org/10.1038/nature12354

Chouhan, A. K., Ivannikov, M. V., Lu, Z., Sugimori, M., Llinas, R. R., & Macleod, G. T. (2012). Cytosolic Calcium Coordinates Mitochondrial Energy Metabolism with Presynaptic Activity. *Journal of Neuroscience*, *32*(4), 1233–1243. https://doi.org/10.1523/JNEUROSCI.1301-11.2012

Consoulas, C., Restifo, L. L., & Levine, R. B. (2002). Dendritic Remodeling and Growth of Motoneurons during Metamorphosis of Drosophila melanogaster. *Journal of Neuroscience*, *22*(12), 4906–4917. https://doi.org/10.1523/jneurosci.22-12-04906.2002

783 Felsenberg, J., Barnstedt, O., Cognigni, P., Lin, S., & Waddell, S. (2017). Re-evaluation of
784 learned information in Drosophila. *Nature*, *544*(7649), 240–244.
785 https://doi.org/10.1038/nature21716

786 Friggi-Grelin, F., Coulom, H., Meller, M., Gomez, D., Hirsh, J., & Birman, S. (2003). Targeted
787 gene expression in Drosophila dopaminergic cells using regulatory sequences from
788 tyrosine hydroxylase. *Journal of Neurobiology*, *54*(4), 618–627.
789 https://doi.org/10.1002/neu.10185

790 Fujii, S., Matsumoto, M., Igarashi, K., Kato, H., & Mikoshiba, K. (2000). Synaptic plasticity in
791 hippocampal CA1 neurons of mice lacking type 1 inositol-1,4,5-trisphosphate receptors.
792 *Learning and Memory*, *7*(5), 312-320. https://doi.org/10.1101/lm.34100

793 Furuichi, T., Kohda, K., Miyawaki, A., & Mikoshiba, K. (1994). Erratum: Intracellular channels
794 (Current Opinion in Neurobiology (1994) 4 (294-303)).. Current Opini*on in*
795 *Neurobiology*, *4*(5), 758. https://doi.org/10.1016/0959-4388(94)90020-5

796 Gomez, L. C., Kawaguchi, S., Collin, T., Jalil, A., Gomez, M. del P., Nasi, E., Marty, A., & Llano,
797 I. (2020). Influence of spatially segregated IP 3 -producing pathways on spike generation
798 and transmitter release in Purkinje cell axons. *Proceedings of the National Academy of*
799 *Sciences*, *117*(20), 11097–11108. https://doi.org/10.1073/pnas.2000148117

800 Handler, A., Graham, T. G. W., Cohn, R., Morantte, I., Siliciano, A. F., Zeng, J., Li, Y., & Ruta, V.
801 (2019). Distinct Dopamine Receptor Pathways Underlie the Temporal Sensitivity of
802 Associative Learning. *Cell*, *178*(1), 60-75. https://doi.org/10.1016/j.cell.2019.05.040

803 Hartenstein, V., Cruz, L., Lovick, J. K., & Guo, M. (2017). Developmental analysis of the
804 dopamine-containing neurons of the Drosophila brain. *Journal of Comparative*
805 *Neurology*, *525*(2), 363–379. https://doi.org/10.1002/cne.24069

806 Hasan, G., & Sharma, A. (2020). Regulation of neuronal physiology by Ca2+ release through
807 the IP3R. *Current Opinion in Physiology*, *17*, 1–8.
808 https://doi.org/10.1016/j.cophys.2020.06.001

809 Inaba, T., Hisatsune, C., Sasaki, Y., Ogawa, Y., Ebisui, E., Ogawa, N., Matsui, M., Takeuchi, T.,
810 Mikoshiba, K., & Tsubota, K. (2014). Mice lacking inositol 1,4,5-trisphosphate receptors
811 exhibit dry eye. PloS one, *9*(6), e99205. https://doi.org/10.1371/journal.pone.0099205

812 James, T. D., Zwiefelhofer, D. J., & Frank, C. A. (2019). Maintenance of homeostatic plasticity
813 at the drosophila neuromuscular synapse requires continuous IP3-directed signaling.
814 *elife*, *8*, e39643. https://doi.org/10.7554/eLife.39643

815 Jayakumar, S., Richhariya, S., Venkateswara Reddy, O., Texada, M. J., & Hasan, G. (2016).
816 Drosophila larval to pupal switch under nutrient stress requires IP3R/Ca2+signaling in
817 glutamatergic interneurons. *ELife*, 5, e17495. https://doi.org/10.7554/eLife.17495

818 Jayakumar, S., Richhariya, S., Deb, B. K., & Hasan, G. (2018). A Multicomponent Neuronal
819 Response Encodes the Larval Decision to Pupariate upon Amino Acid Starvation. *The*
820 *Journal of Neuroscience*, *38*(47), 10202–10219.
821 https://doi.org/10.1523/JNEUROSCI.1163-18.2018

822 Joshi, R., Venkatesh, K., Srinivas, R., Nair, S., & Hasan, G. (2004). Genetic Dissection of itpr
823 Gene Function Reveals a Vital Requirement in Aminergic Cells of Drosophila Larvae.
824 *Genetics*, *166*(1), 225–236. https://doi.org/10.1534/genetics.166.1.225

825 Klose, M. K., Dason, J. S., Atwood, H. L., Boulianne, G. L., & Mercier, A. J. (2010). Peptide-
826 induced modulation of synaptic transmission and escape response in Drosophila
827 requires two G-protein-coupled receptors. *Journal of Neuroscience*, *30*(44), 14724–
828 14734. https://doi.org/10.1523/JNEUROSCI.3612-10.2010

829 Kondo, S., Takahashi, T., Yamagata, N., Imanishi, Y., Katow, H., Hiramatsu, S., Lynn, K., Abe,
830 A., Kumaraswamy, A., & Tanimoto, H. (2020). Neurochemical Organization of the
831 Drosophila Brain Visualized by Endogenously Tagged Neurotransmitter Receptors. *Cell*
832 *Reports*, *30*(1), 284-297. https://doi.org/10.1016/j.celrep.2019.12.018

833 Liu, Q., Liu, S., Kodama, L., Driscoll, M. R., & Wu, M. N. (2012). Two dopaminergic neurons
834 signal to the dorsal fan-shaped body to promote wakefulness in Drosophila. *Current*
835 *Biology*, *22*(22), 2114–2123. https://doi.org/10.1016/j.cub.2012.09.008

836 Lutas, A., Wahlmark, C. J., Acharjee, S., & Kawasaki, F. (2012). Genetic analysis in drosophila
837 reveals a role for the mitochondrial protein P32 in synaptic transmission. *G3: Genes,*
838 *Genomes, Genetics*, *2*(1), 59–69. https://doi.org/10.1534/g3.111.001586

839 Manjila, S., & Hasan, G. (2018). Flight and Climbing Assay for Assessing Motor Functions in
840 Drosophila. *Bio-Protocol*, *8*(5). https://doi.org/10.21769/bioprotoc.2742

841 Megha, & Hasan, G. (2017). IP3R-mediated Ca2+ release regulates protein metabolism in
842 drosophila neuroendocrine cells: Implications for development under nutrient stress.
843 *Development* , *144*(8), 1484–1489. https://doi.org/10.1242/dev.145235

844 Miyata, M., Finch, E. A., Khiroug, L., Hashimoto, K., Hayasaka, S., Oda, S.-I., Inouye, M.,
845 Takagishi, Y., Augustine, G. J., & Kano, M. (2000). Local Calcium Release in Dendritic
846 Spines Required for Long-Term Synaptic Depression. *Neuron*, *28*(1), 233–244.
847 https://doi.org/10.1016/S0896-6273(00)00099-4

848 Nishiyama, M., Hong, K., Mikoshiba, K., Poo, M. M., & Kato, K. (2000). Calcium stores
849 regulate the polarity and input specificity of synaptic modification. *Nature*, *408*(6812),
850 584–588. https://doi.org/10.1038/35046067

851 Ouyang, K., Leandro Gomez-Amaro, R., Stachura, D. L., Tang, H., Peng, X., Fang, X., Traver, D.,
852 Evans, S. M., & Chen, J. (2014). Loss of IP 3 R-dependent Ca 2+ signaling in thymocytes
853 leads to aberrant development and acute lymphoblastic leukemia. *Nature*
854 *Communications*, *5*(1), 1-12. https://doi.org/10.1038/ncomms5814

855 Pang, Z. P., Cao, P., Xu, W., & Südhof, T. C. (2010). Calmodulin controls synaptic strength via
856 presynaptic activation of calmodulin kinase II. *Journal of Neuroscience*, *30*(11), 4132-
857 4142. https://doi.org/10.1523/JNEUROSCI.3129-09.2010

858 Pathak, T., Agrawal, T., Richhariya, S., Sadaf, S., & Hasan, G. (2015). Store-operated calcium
859 entry through Orai is required for transcriptional maturation of the flight circuit in
860 Drosophila. *Journal of Neuroscience*, *35*(40), 13784–13799.

https://doi.org/10.1523/JNEUROSCI.1680-15.2015

Ravi, P., Trivedi, D., & Hasan, G. (2018). FMRFa receptor stimulated Ca2+ signals alter the activity of flight modulating central dopaminergic neurons in Drosophila melanogaster. *PLoS genetics*, *14*(8), e1007459. https://doi.org/10.1371/journal.pgen.1007459

Richhariya, S., Jayakumar, S., Sukumar, S. K., & Hasan, G. (2018). dSTIM and Ral/exocyst mediated synaptic release from pupal dopaminergic neurons sustains drosophila flight. *eneuro*, *5*(3). https://doi.org/10.1523/ENEURO.0455-17.2018

Rossi, B., Maton, G., & Collin, T. (2008). Calcium-permeable presynaptic AMPA receptors in cerebellar molecular layer interneurones. *Journal of Physiology*, *586*(21), 5129–5145. https://doi.org/10.1113/jphysiol.2008.159921

Ryu, C., Jang, D. C., Jung, D., Kim, Y. G., Shim, H. G., Ryu, H.-H., Lee, Y.-S., Linden, D. J., Worley, P. F., & Kim, S. J. (2017). STIM1 Regulates Somatic Ca 2+ Signals and Intrinsic Firing Properties of Cerebellar Purkinje Neurons. *Journal of Neuroscience*, *37*(37), 8876–8894. https://doi.org/10.1523/JNEUROSCI.3973-16.2017

Shakiryanova, D., Morimoto, T., Zhou, C., Chouhan, A. K., Sigrist, S. J., Nose, A., Macleod, G. T., Deitcher, D. L., & Levitan, E. S. (2011). Differential control of presynaptic CaMKII activation and translocation to active zones. *Journal of Neuroscience*, *31*(25), 9093–9100. https://doi.org/10.1523/JNEUROSCI.0550-11.2011

Sharma, G., & Vijayaraghavan, S. (2003). Modulation of presynaptic store calcium induces release of glutamate and postsynaptic firing. *Neuron*, *38*(6), 929–939. https://doi.org/10.1016/S0896-6273(03)00322-2

Sinha, M., & Hasan, G. (1999). Sequencing and exon mapping of the inositol 1,4,5-trisphosphate receptor cDNA from Drosophila embryos suggests the presence of differentially regulated forms of RNA and protein. *Gene*, *233*(1–2), 271–276. https://doi.org/10.1016/S0378-1119(99)00158-4

Sitaraman, D., Aso, Y., Jin, X., Chen, N., Felix, M., Rubin, G. M., & Nitabach, M. N. (2015). Propagation of Homeostatic Sleep Signals by Segregated Synaptic Microcircuits of the Drosophila Mushroom Body. *Current Biology*, *25*(22), 2915–2927. https://doi.org/10.1016/j.cub.2015.09.017

Srikanth, S., & Hasan, G. (2004). Structure and function of inositol 1,4,5-trisphosphate receptors. *Current Science,* 86(11), 1513. Sun, F., Zeng, J., Jing, M., Zhou, J., Feng, J., Owen, S. F., Luo, Y., Li, F., Wang, H., Yamaguchi, T., Yong, Z., Gao, Y., Peng, W., Wang, L., Zhang, S., Du, J., Lin, D., Xu, M., Kreitzer, A. C., … Li, Y. (2018). A genetically encoded fluorescent sensor enables rapid and specific detection of dopamine in flies, fish, and mice. *Cell*, 174(2), 481-496 *Cell*, *174*(2), 481-496.e19. https://doi.org/10.1016/j.cell.2018.06.042

Syed, D. S., Gowda, S. B. M., Reddy, O. V., Reichert, H., & VijayRaghavan, K. (2016). Glial and neuronal Semaphorin signaling instruct the development of a functional myotopic map for Drosophila walking. *ELife*, *5*, e11572. https://doi.org/10.7554/eLife.11572

900 Takei, K., Shin, R. M., Inoue, T., Kato, K., & Mikoshiba, K. (1998). Regulation of nerve growth
901 mediated by inositol 1,4,5-trisphosphate receptors in growth cones. *Science*,
902 *282*(5394). https://doi.org/10.1126/science.282.5394.1705

903 Taylor, C. W., Genazzani, A. A., & Morris, S. A. (1999). Expression of inositol trisphosphate
904 receptors. In *Cell Calcium* 26(6), 237-251. https://doi.org/10.1054/ceca.1999.0090

905 Terry, L. E., Alzayady, K. J., Furati, E., & Yule, D. I. (2019). Inositol 1,4,5-Trisphosphate
906 Receptor Mutations Associated with Human Disease. *Messenger*, *6*(1), 29-44.
907 https://doi.org/10.1166/msr.2018.1075

908 Tsao, C. H., Chen, C. C., Lin, C. H., Yang, H. Y., & Lin, S. (2018). Drosophila mushroom bodies
909 integrate hunger and satiety signals to control innate food-seeking behavior. *ELife*, *7*,
910 e35264. https://doi.org/10.7554/eLife.35264

911 Vicario, D. S., Naqvi, N. H., & Raksin, J. N. (2001). Conditional modification of behavior in
912 Drosophila by targeted expression of a temperature-sensitive shibire allele in defined
913 neurons. *Journal of Neurobiology*, *47*(2), 81–92. https://doi.org/10.1002/neu.1018

914 Xiang, Y., Li, Y., Zhang, Z., Cui, K., Wang, S., Yuan, X. B., Wu, C. P., Poo, M. M., & Duan, S.
915 (2002). Nerve growth cone guidance mediated by G protein-coupled receptors. *Nature*
916 *Neuroscience*, *5*(9), 843–848. https://doi.org/10.1038/nn899

917 Yamazaki, D., Hiroi, M., Abe, T., Shimizu, K., Minami-Ohtsubo, M., Maeyama, Y., Horiuchi, J.,
918 & Tabata, T. (2018). Two Parallel Pathways Assign Opposing Odor Valences during
919 Drosophila Memory Formation. *Cell Reports*, *22*(9), 2346–2358.
920 https://doi.org/10.1016/j.celrep.2018.02.012

921 Zhang, K. X., Tan, L., Pellegrini, M., Zipursky, S. L., & McEwen, J. M. (2016). Rapid Changes in
922 the Translatome during the Conversion of Growth Cones to Synaptic Terminals. *Cell*
923 *Reports*, *14*(5), 1258–1271. https://doi.org/10.1016/j.celrep.2015.12.102

924 Zhang, Y. Q., Rodesch, C. K., & Broadie, K. (2002). Living synaptic vesicle marker:
925 Synaptotagmin-GFP. *Genesis*, *34*(1–2), 142-145. https://doi.org/10.1002/gene.10144

ACKNOWLEDGMENTS

This study was supported by grants from DBT-SERB and NCBS-TIFR to G.H. A.S. was supported by a fellowship from the National Centre for Biological Sciences, TIFR. We thank the Fly Facility, Sequencing facility and Central Imaging and Flow Cytometry Facility at NCBS.